



Quantifying CDOM and DOC in major Arctic rivers during ice-free conditions using Landsat TM and ETM+ data



C.G. Griffin^{a,*}, J.W. McClelland^a, K.E. Frey^b, G. Fiske^c, R.M. Holmes^c

^a Marine Science Institute, University of Texas at Austin, Port Aransas, TX, USA

^b Graduate School of Geography, Clark University, Worcester, MA, USA

^c Woods Hole Research Center, Falmouth, MA, USA

ARTICLE INFO

Keywords:

Chromophoric dissolved organic matter
Dissolved organic carbon
Arctic
Landsat
Remote sensing
Rivers
Google Earth Engine

ABSTRACT

As high-latitudes warm, permafrost thaws, and the hydrological cycle accelerates, ground-based monitoring of riverine organic matter may be supplemented by satellite remote sensing during ice-free conditions. Recent programs, namely the Arctic Great Rivers Observatory, have established methodologically consistent sampling across the hydrograph, and shared the resulting data publicly. However, these efforts are limited by frequency, funding, and length of record. Satellite remote sensing can be used to estimate chromophoric dissolved organic matter (CDOM) as a riverine constituent that influences optical properties in surface waters. In this study, daily CDOM absorption was first estimated using discharge-constituent regression-based models for 2000–2013. We then regressed these discharge-based CDOM estimates against Landsat TM and ETM+ surface reflectance data from Google Earth Engine for the six largest rivers draining the pan-Arctic watershed (the Kolyma, Lena, Mackenzie, Ob', Yenisey, and Yukon rivers). These CDOM results were converted to dissolved organic carbon (DOC), using the strong relationship ($R^2 = 0.88$) between direct measurements of the two constituents. Using river-specific remote sensing models, R^2 could be as high as 0.84. Grouping all rivers into a single “universal” regression reduced R^2 and increased root mean square errors, such as in the Yenisey River where R^2 dropped by 0.63, and RMSE rose by 1.1 m^{-1} . Seasonally varying discharge drove much of the variation in satellite-derived CDOM and DOC, corroborating recent studies. Satellite imagery can increase the frequency of monitoring observations, particularly during summer and fall when riverine CDOM absorption may be most sensitive to thawing permafrost.

1. Introduction

Rivers transport over 3300 km^3 per year of water to the Arctic Ocean, representing $\sim 10\%$ of global riverine discharge annually into an ocean basin containing $\sim 1\%$ of global ocean volume (Aagard and Carmack, 1989; Menard and Smith, 1966). As such, terrestrial processes that impact the delivery of water and water-borne materials have the potential to strongly influence physical, chemical, and biological attributes of the Arctic Ocean. Riverine dissolved organic carbon (DOC) in particular is an important component of the Arctic carbon cycle, linking terrestrial and marine systems (Cooper et al., 2005; Holmes et al., 2012; Manizza et al., 2011). Dissolved organic matter (DOM) in major Arctic rivers is largely allochthonous, sourced from modern vegetation and a smaller fraction from ancient permafrost soils (Guo et al., 2012; Mann et al., 2012; Neff et al., 2006; Raymond et al., 2007). Impacts from rapid climate change, such as thawing permafrost (Frey and

McClelland, 2009; Striegl et al., 2005), an accelerated hydrological cycle (White et al., 2007), and increased fire activity (Elmquist et al., 2008; Stubbins et al., 2015), influence the concentrations and composition of DOM in Arctic rivers. Recent studies have established that DOC from Arctic rivers can be highly labile (Frey et al., 2016; Gustafsson et al., 2011; Mann et al., 2015; Wickland et al., 2012), and losses of river-supplied DOC have been observed along Arctic shelves (Alling et al., 2010). These losses are likely driven by both biological utilization and photochemical interactions with chromophoric dissolved organic matter (CDOM) (Bélanger et al., 2006; Le Fouest et al., 2013; Stedmon et al., 2011), although the relative importance of these processes, and their interactions, remain to be determined. CDOM, the portion of the DOM pool that absorbs light at short wavelengths, is a useful proxy for DOC concentrations in many systems and is important for photochemical transformations (Hu et al., 2002; Spencer et al., 2012).

Although many questions remain about the fate of DOM in the

* Corresponding author.

E-mail address: griffin.claire@gmail.com (C.G. Griffin).

¹ Present address: Department of Ecology, Evolution, and Behavior, University of Minnesota – Twin Cities, Saint Paul, MN, USA.

coastal ocean, coordinated sampling efforts on the six largest Arctic rivers, initiated in 2003 (McClelland et al., 2008), have helped to better constrain estimates of fluvial export. Approximately 35 Tg of DOC is transported by Arctic rivers annually, of which ~15 Tg C are exported by the six largest Arctic rivers during the ice-free seasons (McGuire et al., 2010; Holmes et al., 2012). The Arctic Great Rivers Observatory (Arctic-GRO; 2009–present), originally established as the Pan Arctic River Transport of Nutrients, organic matter, and suspended Sediments (PARTNERS; 2003–2007) project, samples the six largest Arctic rivers across the hydrograph. These rivers – the Kolyma, Lena, Mackenzie, Ob', Yenisey and Yukon – deliver over 50% of annual river discharge and DOC flux to the Arctic Ocean (Holmes et al., 2012). The multi-year datasets from PARTNERS/Arctic-GRO have been used to empirically model fluxes of dissolved and particulate constituents using the USGS Load Estimator (LOADEST) (Holmes et al., 2012; Mann et al., 2016; McClelland et al., 2016). The continued success of this approach, however, is contingent upon long-term funding of water discharge and biogeochemical measurements. LOADEST is a regression-based method that uses discharge-constituent relationships to model fluxes (Runkel et al., 2004), and these relationships can change over time. For example, Tank et al. (2016) defined separate DOC-discharge relationships for each decade to calculate fluxes in the Mackenzie River since the 1980s. Numerous studies in high-latitudes (Larouche et al., 2015) or large river systems (Mann et al., 2014) have tied DOC concentrations or CDOM absorption to important watershed processes (Worrall and Burt, 2010), even when discharge data is unavailable. Satellite remote sensing offers a method of monitoring Arctic rivers that, once established, is independent of discharge.

Satellite imagery has been used over the past decade to map CDOM remotely in a number of optically complex waters (Belanger et al., 2008; Brezonik et al., 2015; Fichot et al., 2013; Kutser, 2012; Menken et al., 2006). Although not originally designed for remote sensing of water quality, the Landsat Thematic Mapper and Landsat Enhanced Thematic Mapper Plus (Landsat TM and ETM+, respectively) have been used to estimate suspended sediment, chlorophyll, turbidity, and CDOM in lakes, rivers and the coastal ocean (Griffin et al., 2011; Joshi and Sa, 2015; Lymburner et al., 2016; Lobo et al., 2015; Olmanson et al., 2008). Landsat TM and ETM+ are limited by lower sensitivity and spectral resolution than ocean colour sensors or newer platforms such as Sentinel-2 or Landsat Operational Land Imager (OLI), making estimations of CDOM difficult in very dark waters with little water-leaving radiance (Kutser et al., 2005; Pahlevan and Schott, 2013; Palmer et al., 2015). Despite these limitations, the high spatial resolution and long-term dataset (1984–present) of Landsat TM and ETM+ make these sensors the best option for monitoring many inland waters (Kutser, 2012).

Here, we present an empirical approach relating CDOM in the six largest Arctic rivers to Landsat reflectance data. The regression-based models presented here represent the first pan-Arctic assessment of DOM in rivers from satellite remote sensing. Using Landsat imagery in conjunction with ground-based measurements of CDOM absorption and DOC concentrations, we estimated CDOM in the six largest Arctic rivers for 424 dates from May through October 2000–2013. We evaluate both “universal” and river-specific regressions, and compare our results to field-based measurements and regression-based discharge constituent models. As well, we examine whether relationships based on temporal variability can be spatially extrapolated.

2. Methods

2.1. Data collection and analysis

Field samples for model development were collected from the Kolyma, Lena, Mackenzie, Ob', Yenisey and Yukon rivers between 2003 and 2013 as part of the Arctic-GRO and PARTNERS projects (Fig. 1; www.arcticgreativers.org). Samples from 2014 to 2016 were used for

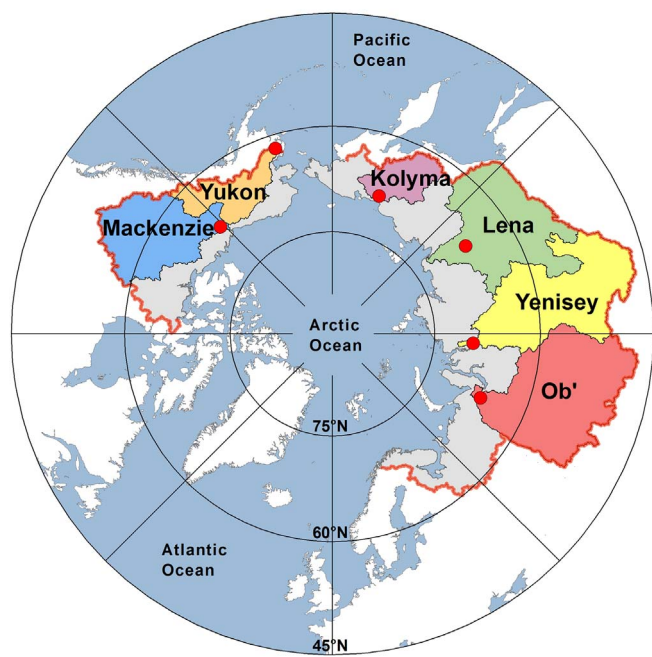


Fig. 1. Map of the Arctic Ocean drainage basin, with the watersheds of the six rivers included in this study. Red points are sampling locations on each river: Ob' at Salekhard, Yenisey at Dudinka, Lena at Zhigansk, Kolyma at Cherskiy, Yukon at Pilot Station, and Mackenzie at Tsiigehtchic. (For interpretation of the references to colour in this figure legend, the reader is referred to the web version of this article.)

independent validation of remote sensing models.

Depth-integrated cross-sectional sampling was conducted at downstream locations on each river, capturing 96% of drainage from their combined watersheds, a total of 10.9 million km² (Holmes et al., 2012). Comparisons of surface samples and depth-integrated samples from the Arctic-GRO/PARTNERS sites have demonstrated that DOC and other dissolved constituents are evenly distributed throughout the water column at these sites (Holmes et al., 2012; Raymond et al., 2007). For more details on sample collection, see previous publications from Arctic-GRO/PARTNERS (Holmes et al., 2012; Raymond et al., 2007; Walker et al., 2013). Sampling campaigns from 2004 to 2011 explicitly addressed the highly seasonal nature of Arctic rivers, with targeted sampling during spring freshet, throughout the ice-free period, and during winter under the ice (McClelland et al., 2008). From 2012 – present, sampling occurred on each river every other month. Additional samples, used in this study for further model evaluation, were collected during field campaigns to the Mackenzie (2011) and Kolyma (2013) rivers, in the spring shortly after ice break-up on each river. These surface samples, from approximately 0.5 m depth, were collected and stored in polycarbonate or HDPE bottles, 1–2 L volume, and processed within hours of collection.

Arctic-GRO and PARTNERS DOC and CDOM samples were filtered within 2–4 h of sample collection through 0.45 μm Geotech medium or high capacity capsule filters into pre-cleaned, pre-rinsed HDPE bottles and shipped frozen to the Woods Hole Research Center (WHRC). DOC samples from PARTNERS (2003–2006) were measured for concentration at the National Ocean Sciences Atomic Mass Spectrometry (AMS) facility at Woods Hole Oceanographic Institute or the AMS facility at University of Arizona (Holmes et al., 2012; Raymond et al., 2007). All Arctic-GRO DOC samples were measured at the WHRC using a Shimadzu (TOC-V) organic carbon analyzer. Absorbance was measured at WHRC using a dual-beam Shimadzu UV-1800 with a 1 cm quartz cuvette, from wavelengths 200–800 nm at 1 nm intervals against nanopure water with ± 0.4%. Owing to logistical constraints, these measurements were made using frozen water samples which can lead to changes

Table 1

LOADEST model coefficients and R² values from Model 6 (see [Methods](#)), used to develop daily CDOM absorption and DOC concentration estimates, ± standard error. Statistically significant coefficients are marked with an asterisk (*).

River	Coefficients ± 1 standard deviation					R ² (%)
CDOM	a ₀	a ₁	a ₂	a ₃	a ₄	
Kolyma	1.56 ± 0.20*	0.50 ± 0.09*	-0.003 ± 0.05	-0.55 ± 0.26*	0.28 ± 0.14*	73
Lena	2.56 ± 0.11*	0.45 ± 0.05*	-0.02 ± 0.05	-0.53 ± 0.13 *	0.40 ± 0.09*	89
Mackenzie	1.47 ± 0.31*	1.58 ± 0.43*	0.06 ± 0.45	1.00 ± 0.31*	-0.77 ± 0.37*	53
Ob'	2.62 ± 0.24*	0.53 ± 0.13*	-0.17 ± 0.28	-0.30 ± 0.21	-0.16 ± 0.18	45
Yenisey	1.83 ± 0.19*	0.59 ± 0.13*	0.25 ± 0.14	0.37 ± 0.20	-0.29 ± 0.13*	72
Yukon	1.66 ± 0.23*	1.01 ± 0.17*	-0.15 ± 0.18	-0.57 ± 0.27*	0.58 ± 0.19*	70
DOC	a ₀	a ₁	a ₂	a ₃	a ₄	
Kolyma	1.82 ± 0.16*	0.41 ± 0.07*	-0.03 ± 0.04*	-0.67 ± 0.20*	-0.07 ± 0.10*	64
Lena	2.38 ± 0.12*	0.33 ± 0.06*	-0.03 ± 0.05	-0.57 ± 0.14 *	-0.42 ± 0.08	74
Mackenzie	1.43 ± 0.12*	0.18 ± 0.15*	0.17 ± 0.17*	0.08 ± 0.16	-0.04 ± 0.08	31
Ob'	2.33 ± 0.13*	0.18 ± 0.07*	-0.17 ± 0.15*	-0.03 ± 0.12	-0.07 ± 0.09*	43
Yenisey	1.74 ± 0.10*	0.39 ± 0.08*	0.06 ± 0.08*	0.29 ± 0.11*	-0.07 ± 0.08*	75
Yukon	1.63 ± 0.13*	0.78 ± 0.09*	-0.08 ± 0.10*	-0.50 ± 0.15*	0.37 ± 0.10*	80

in CDOM as ice excludes organic matter ([Belzile et al., 2002](#); [Peacock et al., 2015](#)). The remote nature of these regions necessitated sample storage, however, and others have found minimal effects of freezing on DOM (([Spencer and Coble, 2014](#)) and references therein). Whole water samples were shipped to the Marine Biological Laboratory for total suspended sediment (TSS) analyses. These samples were filtered onto pre-weighed Whatman GF/F filters and weighed after drying for 24 h at 60 °C. The volume of water passing through each filter was recorded, and TSS concentrations were calculated from the paired mass and volume data.

Additional field samples from the Mackenzie watershed in 2011 and Kolyma watershed in 2013 were also filtered through 0.45 µm Geotech capsule filters into pre-cleaned, pre-rinsed polycarbonate bottles. CDOM was measured immediately after filtration using a single-beam Ocean Optics USB4000 UV-VIS spectrophotometer on the Mackenzie River in 2011. A dual-beam Shimadzu UV-1800 located at the Northeast Science Station in Cherskiy, Russia was used for CDOM in 2013 for Kolyma river samples. In both cases, absorbance was measured within 24 h of collection, from 200 to 800 nm through a 1 cm quartz cuvette, with blank-correction using nanopure water. Samples for Mackenzie (2011) DOC concentration measurements were frozen and shipped to WHRC for analysis. Kolyma samples from 2013 were stored frozen until analyzed with a Shimadzu (TOC-V) at the Northeast Science Station. Absorbance was converted to absorption coefficients using Eq. 1:

$$a(\lambda) = 2.303A(\lambda)/l \quad (1)$$

where $a(\lambda)$ is the absorption coefficient at a given wavelength, $A(\lambda)$ is the absorbance at a given wavelength, and l is the path length in meters ([Hu et al., 2002](#)). Absorption at 375 nm was used for subsequent LOADEST modeling and remote sensing applications, as full absorbance scans were not available for PARTNERS data from 2003 to 2006. Chlorophyll, which also can influence remotely sensed CDOM estimates, is generally low in large Arctic rivers ([Emmerton et al., 2008](#); [Meon and Amon, 2004](#)).

2.2. LOADEST modeling

Despite the rich dataset provided by PARTNERS and Arctic-GRO, there were only 8–25 instances per river where ground sampling corresponded to ≤3 days of an ice-free and cloud-free Landsat satellite overpass from 2003 to 2013. Landsat sensors (Landsat 5 TM and Landsat 7 ETM+, in this study) are high resolution (30 m) multispectral sensors with a 16 day return interval. Because Landsat sensors are polar-orbiting, 2–3 scenes overlap any particular point at high latitudes, allowing more frequent overpasses for each sampling site. Still, the frequency of clouds and long ice-covered season limit the number of

suitable scenes available and there are only ~4–5 samples from the field available per river annually during the open water season.

To address this limitation in available field data, we estimated daily CDOM absorption for 2000–2013 using LOADEST. LOADEST has been used in multiple studies to estimate concentrations and fluxes of biogeochemical parameters based on PARTNERS and Arctic-GRO data ([Holmes et al., 2012](#); [Mann et al., 2016](#); [Raymond et al., 2007](#); [Tank et al., 2012](#)), and other studies of CDOM flux ([Spencer et al., 2013](#)). LoadRunner version 2.1 (<http://environment.yale.edu/loadrunner>) was used to automate LOADEST runs.

Discharge data were collected by the USGS (Yukon), Water Survey of Canada (Mackenzie), and Roshydromet (Federal Service for Hydrometeorology and Environmental Monitoring in Russia; Kolyma, Lena, Ob' and Yenisey). The Yukon River includes discharge data from 2001 to 2013, the Mackenzie River includes discharge data from 2000 to 2012, and all other rivers include discharge data from 2000 to 2013. On the Ob', Yukon and Mackenzie rivers, discharge gauging stations coincide with biogeochemical constituent collection locations. On the Yenisey and Kolyma, gauging stations are 160 km and 250 km upstream of constituent sampling, respectively. Discharge gauging occurs 520 km downstream of constituent sampling on the Lena. We used corrections of 1 (Yenisey), 2 (Kolyma) and 4 (Lena) days to account for the lag times between gauging and sample collection ([Holmes et al., 2012](#)), which were applied before running LOADEST (Table 1).

LOADEST model 6 (Eq. 2, below), was used to estimate daily CDOM absorption and DOC concentration. This model includes terms that account for seasonality (the terms with sine and cosine functions) as well as variation in discharge.

$$\begin{aligned} \text{Ln}(\text{Conc}) = & a_0 + a_1 \text{Ln}Q + a_2 \text{Ln}Q^2 + a_3 \text{Sin}(2\pi d_{\text{time}}) \\ & + a_4 \text{Cos}(2\pi d_{\text{time}}) \end{aligned} \quad (2)$$

where Q is water discharge in cubic feet per second, $\text{Ln}Q$ equals $\text{Ln}(Q)$ minus center of $\text{Ln}(Q)$, and d_{time} is decimal time minus center of decimal time. The centering procedure for both discharge and time is used to avoid multicollinearity. Concentration (Conc) is reported in units of m^{-1} for CDOM and as mg/L for DOC. Concentration or absorption estimates are from the adjusted maximum likelihood output of LOADEST.

2.3. Landsat image processing

We used the Landsat Ecosystem Disturbance Adaptive Processing System (LEDAPS, Version 2) data from Google Earth Engine (GEE) ([Gorelick et al., 2017](#)), which calculates surface reflectance for Landsat 5 TM and 7 ETM+ ([Hansen et al., 2013](#); [Masek et al., 2006](#)). Landsat provides a thorough, consistent record of these rivers across the entire study time period (2000–2013). Other sensors, such as the Advanced

Land Imager (ALI) or MODerate resolution Imaging Spectroradiometer (MODIS), would provide improved radiometric sensitivity but lack recurring clear sky imagery or spatial resolution to monitor these rivers. GEE is a relatively new cloud-based platform that allows for on-the-fly processing of remotely sensed data. Using GEE, downloading hundreds of satellite images for analyses is no longer necessary and image processing can be quickly automated. This is the first study that we know of using GEE for remote sensing of water quality parameters in inland waters. Previous GEE studies demonstrated its use for regional to global scale analyses through time for applications including forest and land use change (Hansen et al., 2013) and global surface water distribution (Pekel et al., 2016), and resource use impacts on groundwater (Huntington et al., 2016).

LEDAPS, also a data product from USGS, applies the 6S radiative transfer model (Second Simulation of a Satellite Signal in the Solar Spectrum) to ortho-rectified Landsat data, with auxiliary ozone data from the NASA GSFC Ozone Monitoring Instrument or Total Ozone Mapping spectrometer and gridded atmospheric data from the National Centers for Environmental Prediction (NCEP) (Masek et al., 2006; Schmidt et al., 2013). Surface reflectance is further corrected using an internal Aerosol Optical Thickness (AOT) parameter, based on Dense, Dark Vegetation (DDV) and the correlation of reflectance between the blue and red bands (Claverie et al., 2015; Kaufman et al., 1997). Previous studies have shown that the LEDAPS method of calculating AOT is comparable to retrievals from the Aerosol Robotic Network (AERONET) and MODIS (Claverie et al., 2015; Maersperger et al., 2013). This method does not account for Fresnel reflectance, the scattering of light at the air-water interface resulting from differences in refraction. A number of recent papers have used similar approaches in the remote sensing of water quality, including remote sensing of Secchi depth (Rodrigues et al., 2017) and CDOM (Slonecker et al., 2016). The USGS Surface Reflectance Product was designed to be on a global scale, for a wide variety of environments. We also compared LEDAPS data to Top-of-Atmosphere (TOA) radiance (Kutser, 2012) (Fig. S2) for the Lena and Yenisey rivers. Additionally, an initial investigation of the Arctic-GRO samples compared to Landsat data corrected by ENVI Fast Line-of-sight Atmospheric Analysis of Hypercubes (FLAASH) showed promising results (Fig. S3). However, this approach was limited by the small number of on the ground samples, as discussed in Section 2.2. Additionally, FLAASH is not easily automated, and given the lack of concurrent ground-based atmospheric measurements, we could only use a generic “boreal” model, rather than the ancillary data that is used by LEDAPS.

Over 420 Landsat TM and ETM+ scenes from 2000 to 2013 were used in the remote sensing analyses (Table 2; Fig. 2). We used scenes with 30% or less cloud cover, all with clear-sky conditions over sampling locations. Only scenes from May 15th – October 15th were included, with scenes from shoulder seasons visually inspected to insure no interference from floating ice. A 3-pixel-wide cross-section at the sampling site for each river was digitized and used to extract mean reflectance for the area of interest (AOI), corresponding to the cross-sectional sampling design of Arctic-GRO. In images from Landsat 7 ETM

Table 2

Number of Landsat scenes used to develop regression equations between CDOM absorption and remote sensing reflectance data. Scenes are from 2000 to 2013.

River	Landsat scenes used			
	Freshet	Summer	Fall	Total
Kolyma	25	35	8	68
Lena	19	38	14	71
Mackenzie	50	47	14	111
Ob'	23	33	19	75
Yenisey	10	38	7	55
Yukon	14	19	11	44
Total	141	210	73	424

+ post-2003, a failure of the Scan Line Corrector (SLC) caused data gaps in each image; however, because each cross section spans hundreds of meters in these large rivers, data were missing from only ~25% or less of the AOI in these scenes. We extracted reflectance from Landsat bands 1 (blue; 450–520 nm), 2 (green; 520–600 nm), 3 (red; 630–690 nm), and 4 (near infrared; 760–900 nm). River masks were created using the Hansen et al. (2013) dataset which includes a water layer. A simple cloud score method based on the thermal band removed clouds (Hansen et al., 2013).

Samples from 2011 and 2013, collected separately from the main Arctic-GRO sampling, were used to evaluate whether regression models based upon temporal variability could be extrapolated across space. These samples came from main stem, tributary, and channel locations within the Mackenzie and Kolyma drainage basins. Samples were collected shortly after ice breakup on each river, within a 2–4 week period. In the Mackenzie, most samples that corresponded with cloud-free Landsat imagery were collected from channels in the extensive delta, and a handful of samples from tributaries or the main stem of the river. Kolyma river samples were more evenly split, with five samples from major tributaries and four samples from different sections of the main stem of the river. Only samples from channels 90 m wide or more are used here, to avoid edge effects. AOIs consisted of a 30 m buffer around each sampling point, from which reflectance was extracted. In cases where samples were collected from shore, AOIs were artificially moved towards the river center to avoid edge effects, on the assumption that DOM was well-mixed within the river. In the Mackenzie River, all but one sample was collected on the same day as a satellite fly-over. A June 18th, 2011 sample from the main stem of the river at Tsiigehtchic was offset from Landsat imagery by one day, and discharged varied between the two days by < 1%. Sample collection and satellite overpass in the Kolyma watershed was within ± 3 days. While we do not have discharge data from Kolyma tributaries to assess their dynamics, discharge at the main stem of the Kolyma near Cherskiy varied by < 3% between dates of sample collection and Landsat overpass. The relative stability of discharge indicates that the main pulse of spring freshet has passed by the time these samples were collected, and that CDOM dynamics have slowed. After applying river-specific regression models from Table 3, Landsat-derived CDOM values were compared to on-the-ground measurements.

An additional validation was performed using atmospherically corrected Landsat 7 and 8 data from 2014 to 2016 for all rivers, plus 2013 data from the Mackenzie River. We used cloud and ice-free imagery that matched within 3 days of Arctic-GRO field collection. After applying the river-specific equations developed above, we compared remotely estimated CDOM and DOC to measured Arctic-GRO data for 18 dates. These data were not used in developing LOADEST models, and represent an independent evaluation of the performance of our models.

2.4. Statistical analysis

All statistical analyses were performed in R software (<https://www.r-project.org/>). Although we might expect CDOM to have the largest effect on reflectance in the blue band (B1) of Landsat, given the exponential decrease in CDOM absorption as wavelength increases from 200 to 800 nm, most previous studies depend on a combination of the green and red bands (B2 and B3) (Joshi and Sa, 2015; Kallio et al., 2008; Kutser, 2012). Some previous studies had success using B1 and B4 (near infrared band; NIR), as well (Brezonik et al., 2005; Griffin et al., 2011; Olmanson et al., 2016). Bands 1–4 and band ratios were tested in exhaustive iterations of linear and multiple linear regressions against the LOADEST CDOM a_{375} results, grouped by river (Table 3). Additionally, we performed the same analysis with all data grouped together to determine whether a more universal model could be used on a pan-Arctic scale (Table 3). All Landsat CDOM values reported hereafter refer to absorption at 375 nm. Multiple linear regressions

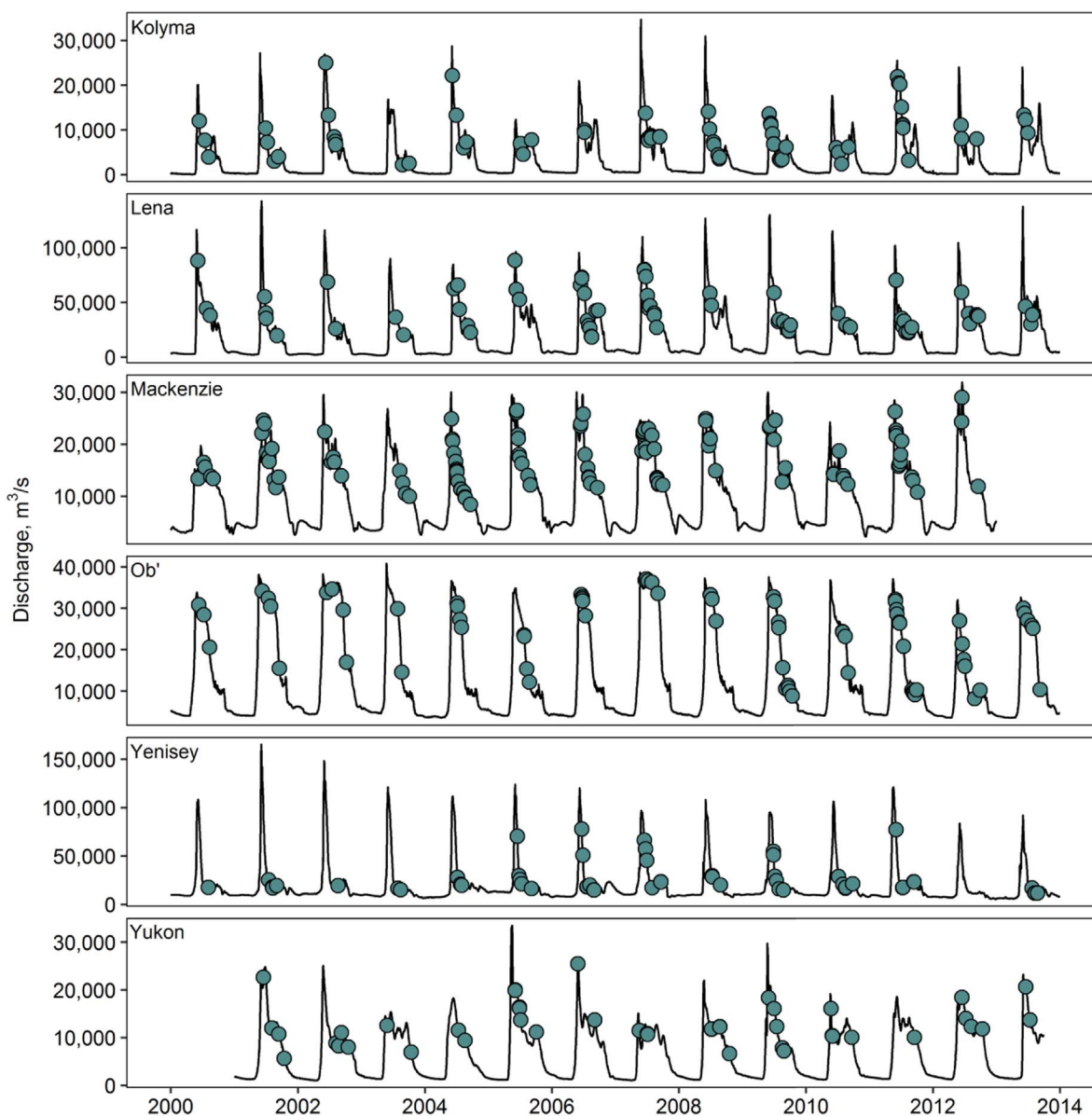


Fig. 2. Daily discharge for each river from 2000 to 2013. Blue dots indicate dates of Landsat data used in regressions between LOADEST-derived CDOM and surface reflectance. (For interpretation of the references to colour in this figure legend, the reader is referred to the web version of this article.)

ultimately were the most successful, evaluated based on Schwartz's Bayesian Information Criteria (BIC) and R^2 . BIC includes a penalty term for increasing the number of variables in a regression in order to avoid overfitting; while useful for model selection, BIC is not generally used to compare between different datasets. If BIC and R^2 were similar between differing models for the same river system, the model with only one band ratio or the least number of variables was selected. We compared differences in CDOM between three methods (Arctic-GRO measurements, LOADEST estimates, and Landsat-derived estimates) during the ice-free season. Cross-sectional river sampling is dangerous during the spring break-up and autumn freeze periods, so all field-collected samples from May to mid-October are assumed to be ice-free. We assumed that rivers would be ice-free from three days after peak discharge until October 15th. Average absorptions and concentrations for seasonal and total ice-free periods were calculated for 2004–2006 and 2009–2012, the common years between all three methods. Mean seasonal absorptions and concentrations were averaged together for the total ice-free period, so that seasons were given equal weight despite differences in coverage between methods.

3. Results

3.1. DOM measurements and LOADEST modeling

CDOM absorption is a common proxy for DOC concentrations in inland waters, including Arctic rivers (Frey et al., 2016; Osburn and Stedmon, 2011; Stedmon et al., 2011). Using all available Arctic-GRO data from 2004 to 2014, DOC and a_{375} correlate strongly across all rivers (Fig. 3 and Eq. 3; $R^2 = 0.88$, $n = 248$, ordinary least squares regression):

$$\text{CDOM} = 1.593 \cdot \text{DOC} - 2.453 \quad (3)$$

where CDOM is the absorption coefficient at 375 nm and DOC is the concentration of DOC in mg/L, using ordinary least squares regression. DOC ranges from 2.1 mg/L C to 23.5 mg/L C with a mean of 7.6 mg/L C; CDOM a_{375} ranges 1.1 m^{-1} to 29.7 m^{-1} with a mean of 9.7 m^{-1} .

The ability of LOADEST to predict CDOM a_{375} (based on R^2 values of regression relationships) in the six Arctic-GRO rivers ranged from 0.45 to 0.89, using Model 6 (Table 1). Of these, LOADEST models for the Ob' and Mackenzie rivers are the least predictable with R^2 of 0.45

Table 3

Landsat multispectral bands used to develop relationships between CDOM and reflectance for each river based on both river-specific and universal regressions, and the respective R^2 , root mean square error (RMSE), mean absolute percent difference (MAPD) \pm the MAPD standard deviation, and the range of a_{375} values from LOADEST input and Landsat output.

Landsat bands	Equation coefficient				LOADEST			Landsat		
	$a_{375} = b_0 + b_1(x_1) + b_2(x_2) + b_3(x_3)$				R^2	RMSE	MAPD	CDOM range		
	Combinations	b_0	b_1	b_2	b_3	(m^{-1})	(%)	(m^{-1})	(m^{-1})	
River-specific models										
Kolyma	ln(B2), ln(B3), B2/B3	-25.877	-73.114	71.126	46.59	0.73	1.48	17.7 \pm 16.3	2.88–14.99	2.44–12.36
Lena	ln(B3), ln(B4), ln(B2/B4)	74.757	23.695	-33.051	-42.469	0.67	2.96	18.6 \pm 13.3	7.25–28.16	6.25–23.11
Mackenzie	ln(B2), B4	93.7	-14.1	0.00938		0.53	1.45	23.4 \pm 18.2	2.16–11.43	2.73–9.09
Ob'	B1, B2/B3	20.979	0.0004081	-6.9707		0.33	1.21	6.1 \pm 6.6	9.56–19.00	11.36–15.53
Yenisey	ln(B2), ln(B3), B2/B3	-76.721	-151.4	151.24	97.766	0.84	1.17	8.8 \pm 7.9	7.56–20.59	7.64–19.09
Yukon	B1, B2, B1/B4	38.709	0.026741	0.03664	-17.568	0.75	2.33	28.1 \pm 27.0	3.55–19.55	-0.64–15.60
All Rivers						0.85	1.84	17.2 \pm 17.3	2.16–28.16	-0.64–23.11
Universal model										
Kolyma						0.53	2.09	27.7 \pm 25.9	2.88–14.99	0.75–11.38
Lena						0.65	4.32	19.9 \pm 13.9	7.25–28.16	8.40–15.42
Mackenzie						0.41	2.88	52.9 \pm 49.9	2.16–11.43	-8.80–13.13
Ob'						0.06	3.2	15.3 \pm 16.1	9.56–19.00	1.11–17.85
Yenisey						0.21	2.72	21.5 \pm 14.8	7.56–20.59	4.03–13.54
Yukon						0.27	4.01	44.6 \pm 60.6	3.55–19.55	-7.03–16.91
All Rivers	B2, B3, B2/B3	32.475	-0.0257	0.01659	-14.621	0.52	3.23	31.8 \pm 38.1	2.16–28.16	-8.80–17.85

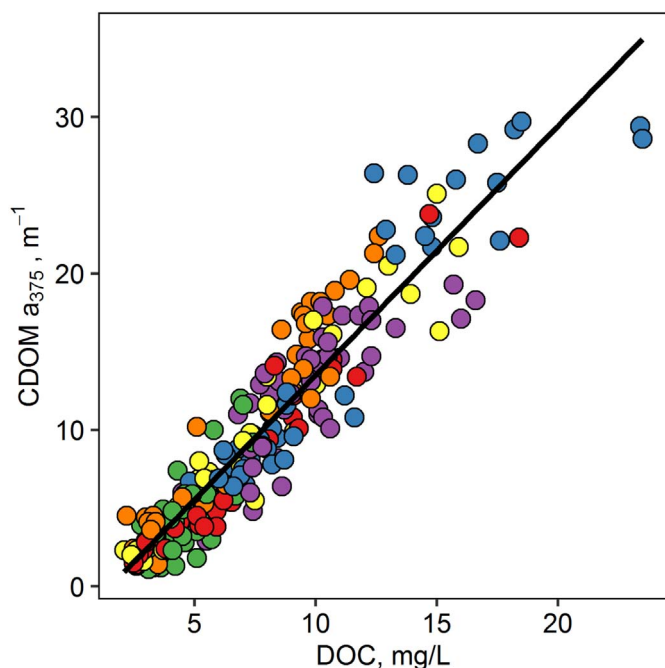


Fig. 3. Regression between measured DOC and CDOM a_{375} , from the Arctic-GRO dataset from 2004 to 2014. $CDOM = 1.59 * DOC - 2.45$; $R^2 = 0.88$; $RMSE = 2.31 m^{-1}$, $n = 248$. Red = Kolyma, Green = Mackenzie, Orange = Yenisey, Blue = Lena, Purple = Ob', Yellow = Yukon. (For interpretation of the references to colour in this figure legend, the reader is referred to the web version of this article.)

and 0.53, respectively. CDOM predicted by LOADEST Model 6 resulted in R^2 of 0.70–0.73 for the Yukon, Yenisey, and Kolyma, and 0.89 for the Lena river. Here, model coefficients a_0 (the intercept) and a_1 (related to discharge) are significant and a_2 (natural log of discharge squared) is non-significant for all rivers. Coefficient a_3 , a seasonality parameter, is significant for the Kolyma, Lena, Mackenzie, and Yukon rivers and non-significant for the Ob' and Yenisey. With the exception of the Ob', coefficient a_4 , also a seasonality parameter, is significant for all rivers.

LOADEST modeling of DOC concentrations explain overall less variance than the CDOM models, with the largest divergence in the Mackenzie where R^2 values drops from 0.53 to 0.31. The Lena also shows a sizable drop, with R^2 values decreasing from 0.89 to 0.74. The

Yukon River is the exception, with R^2 increasing from 0.70 to 0.80 between CDOM and DOC models. Although this paper presents DOC concentrations derived from remote sensing, we chose to use LOADEST-derived CDOM as calibration data for remote sensing models because of this difference in explanatory power, in addition to CDOM being a more direct measure of the spectral characteristics of water bodies (Brezonik et al., 2015).

3.2. Landsat regression models of CDOM and DOC

Our results indicate that CDOM, can be estimated using Landsat TM and ETM+ data (Fig. 4), as well as DOC by applying Eq. 3 to the remotely estimated CDOM values. Using river-specific regressions from Table 3, CDOM a_{375} from Landsat data correlates with LOADEST-derived CDOM a_{375} with an overall R^2 of 0.85. DOC estimates from Landsat correlate with LOADEST-derived DOC with an overall R^2 of 0.74. A universal regression, using all rivers grouped into one dataset, resulted in a decreased R^2 of 0.52 (Table 3). Individual rivers also decreased markedly in R^2 using this universal approach, while RMSE increased with particularly dramatic changes in the Yenisey and Yukon rivers (Table 3; Fig. S1). Using the Landsat TOA product, instead of surface reflectance models, also resulted in a decreased R^2 and increased RMSE (Fig. S2). The Lena River R^2 decreased from 0.67 to 0.49, and RMSE increased from $2.96 m^{-1}$ to $3.89 m^{-1}$. The Yenisey River R^2 decreased from 0.84 to 0.61 and RMSE increased from 1.17 to $2.05 m^{-1}$.

Although our overall ability to predict CDOM in large Arctic rivers is comparable to other studies using Landsat (e.g., Kutser et al., 2005; Kallio et al., 2008; Olmanson et al., 2016), regression models vary widely between each river in terms of formulation and performance (Table 3). The Yenisey performs best, with a R^2 of 0.84 and root mean square error (RMSE) of $1.17 m^{-1}$. CDOM models for the Yenisey and the Kolyma are the only two cases that share the same band variables, a combination of the log-transformed green and red bands with a ratio of green to red (Table 3). The Ob' regression also uses a ratio of green to red, in combination with the blue band, and has a RMSE that is comparable to the other rivers, but its R^2 is only $0.33 m^{-1}$. The Yukon River model uses the blue band, green band, and a ratio of the blue and NIR bands and explains 75% of the variance in CDOM and RMSE of $2.33 m^{-1}$. The Lena model uses natural log-transformed red and NIR bands with a natural-log of the green to NIR band ratio, resulting in a R^2 of 0.68 and RMSE of $2.96 m^{-1}$. The Mackenzie River model is the only

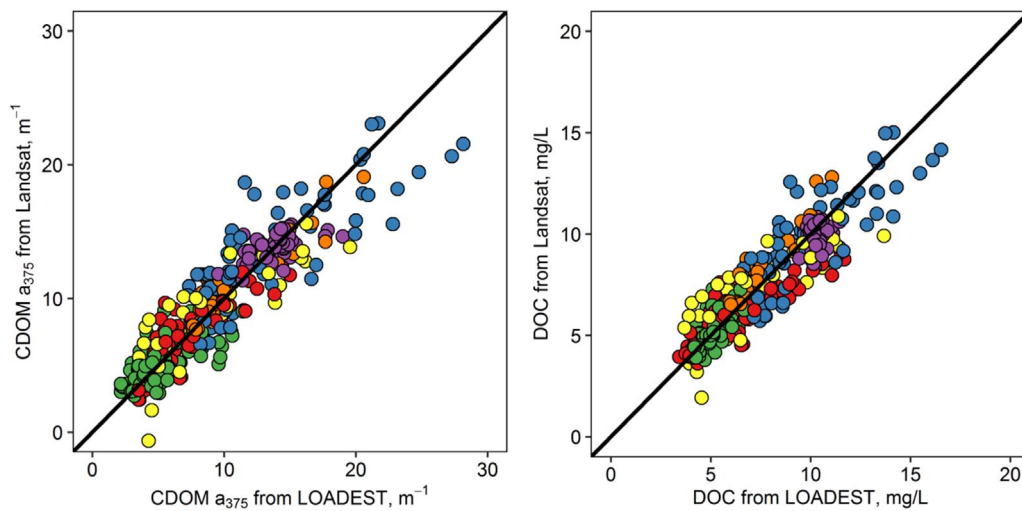


Fig. 4. Scatterplots of CDOM and DOC from LOADEST compared to remote sensing estimates, using river-specific regressions. The line in both plots is one-to-one. Individual river regressions vary, but overall CDOM is predicted with $R^2 = 85\%$, DOC with $R^2 = 74\%$. Red = Kolyma, Green = Mackenzie, Orange = Yenisey, Blue = Lena, Purple = Ob', Yellow = Yukon. (For interpretation of the references to colour in this figure legend, the reader is referred to the web version of this article.)

model that does not include a band ratio, instead using the NIR and natural log of the green band for a R^2 of 0.53 and RMSE of 1.45 m^{-1} .

3.3. Spatial evaluation

CDOM in the Kolyma main stem samples fall close to the one-to-one line, despite spanning almost 300 km along the river (Figs. 5 and 6). CDOM estimates from tributaries of the Kolyma were less consistent, although three observations were within 1 m^{-1} of measured values (Fig. 6). When converted to DOC, seven out of nine Landsat-derived estimates were within 1.1 mg/L C of measured DOC concentrations. The Mackenzie remote sensing model, on the other hand, did not yield reliable estimates of CDOM or DOC across space. Although measured CDOM a_{375} ranges by nearly 20 m^{-1} in the Mackenzie, our remote sensing model could not capture that variability. Remotely sensing methods underestimated CDOM in the Mackenzie delta and could not capture the range of variability observed in measured data. For the eight samples within the delta where Landsat imagery corresponds within 3 days \pm of field sampling, measured a_{375} averages $14.94 \pm 4.29 \text{ m}^{-1}$ while remote sensing estimates average $5.77 \pm 1.27 \text{ std. m}^{-1}$. Samples of the Mackenzie main stem and major tributaries upstream of the delta matched somewhat more closely with measured a_{375} averaging $8.62 \pm 2.44 \text{ m}^{-1}$ and estimated a_{375} averaging $7.26 \pm 0.18 \text{ m}^{-1}$.

3.4. Comparing measured, LOADEST, and Landsat DOM

To compare CDOM and DOC between methods (Arctic-GRO, LOADEST, and Landsat) we only included 2004–2006 and 2009–2012, the years when all three approaches have complete seasonal datasets (Table 4). Discharge data for all rivers was not available in 2000 or 2013, and PARTNERS/Arctic-GRO did not sample in 2007 and 2008. Landsat-derived CDOM estimates are available for these years where LOADEST or Arctic-GRO have gaps, but are not considered in Table 4. Remotely sensed estimates of seasonal CDOM and DOC show little significant difference from either measured or LOADEST values, in most rivers (Table 4). During freshet (May–June), average measured CDOM and DOC are significantly higher than Landsat estimates for the Lena and Kolyma rivers. Average LOADEST DOC during freshet on the Kolyma also significantly exceeds Landsat estimated DOC. Freshet in the Lena exhibits the largest divergence between methods for any season on any river, with average measured CDOM and DOC exceeding Landsat estimates by 6.61 m^{-1} and 3.55 mg/L , respectively. In the Ob' River, average Landsat DOC concentrations in summer are significantly lower than measured or LOADEST values. Measured CDOM in the Ob' River during fall is significantly lower than Landsat CDOM. However, LOADEST DOC is significantly higher than Landsat DOC for the same season in the Ob'. During summer in the Yukon River, average CDOM from Landsat is significantly higher than LOADEST values, and Landsat-

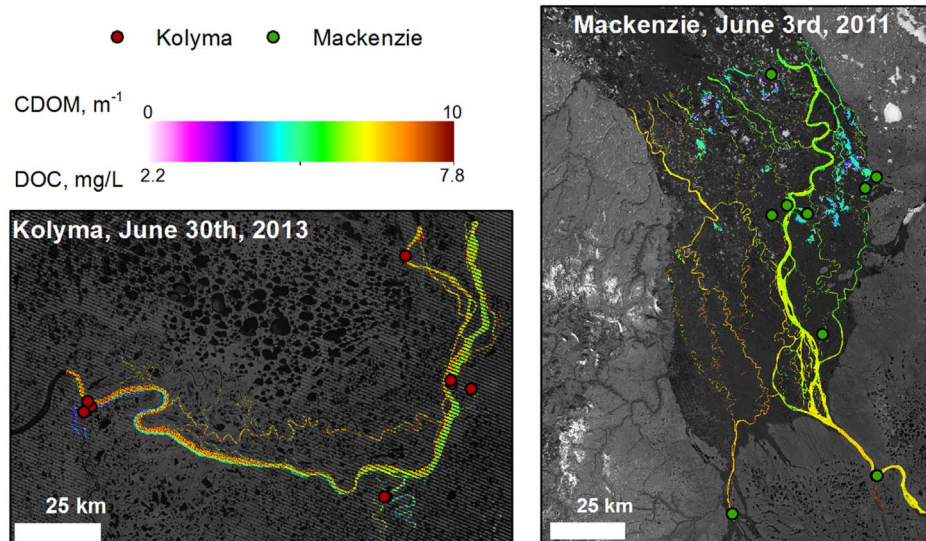


Fig. 5. Map of CDOM a_{375} and DOC from remote sensing for the Kolyma and Mackenzie rivers, with sampling sites used for spatial evaluation. Imagery corresponds to field campaigns (Mackenzie in June 2011, Kolyma in June–July 2013). Red points = Kolyma, Green points = Mackenzie. (For interpretation of the references to colour in this figure legend, the reader is referred to the web version of this article.)

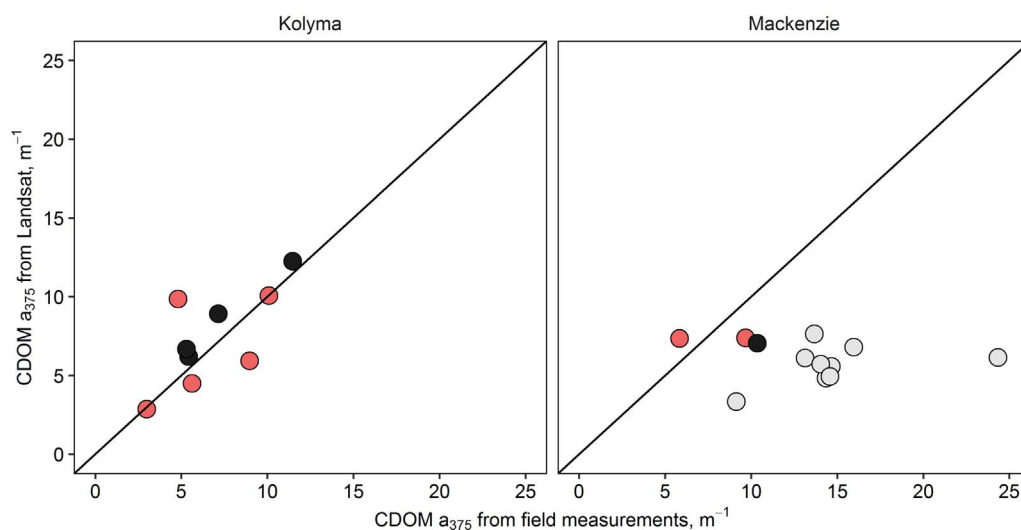


Fig. 6. Comparison of field collected CDOM measurements and Landsat-derived estimates, from samples distributed across the lower watersheds of the Kolyma and Mackenzie rivers. Line is one-to-one. Grey = delta, Black = main stem, Pink = tributary. (For interpretation of the references to colour in this figure legend, the reader is referred to the web version of this article.)

Table 4

Average a_{375} and DOC concentrations for the ice-free period from three data sources, for 2004–2006 and 2009–2012. Seasonal averages were calculated for the entire time period, \pm standard error. Total ice-free period absorptions and concentrations are averages of the seasonal values, so that equal weight is given to each season. Landsat-derived seasonal means were compared to measured and LOADEST values using Tukey's post hoc test ($p = 0.05$). Italics indicates significant difference from measured data and bold indicates significant difference from LOADEST results. CDOM units are $a_{375} \text{ m}^{-1}$. DOC is in mg/L C.

	Freshet			Summer			Fall			Total Ice-free Period	
	CDOM	DOC	n	CDOM	DOC	n	CDOM	DOC	n	CDOM	DOC
Kolyma											
Measured	12.1 \pm 1.54	9.65 \pm 0.99	14	5.70 \pm 0.83	5.51 \pm 0.62	6	4.00 \pm 0.32	4.42 \pm 0.44	7	7.25 \pm 2.45	6.53 \pm 1.59
LOADEST	9.42 \pm 0.2	8.46 \pm 0.13	172	4.95 \pm 0.07	5.06 \pm 0.05	434	5.21 \pm 0.06	5.59 \pm 0.05	280	6.53 \pm 1.45	6.37 \pm 1.06
Landsat	8.75 \pm 0.61	7.1 \pm 0.34	15	5.89 \pm 0.44	5.53 \pm 0.24	17	6.59 \pm 0.57	5.92 \pm 0.32	4	7.08 \pm 0.86	6.18 \pm 0.47
Lena											
Measured	25.6 \pm 0.87	16.3 \pm 0.77	14	9.23 \pm 0.76	7.41 \pm 0.46	5	8.23 \pm 0.31	7.26 \pm 0.26	7	14.4 \pm 5.62	10.3 \pm 2.98
LOADEST	20.1 \pm 0.29	13.2 \pm 0.12	178	10.6 \pm 0.11	8.46 \pm 0.06	434	9.55 \pm 0.07	8.18 \pm 0.04	280	13.4 \pm 3.34	9.93 \pm 1.61
Landsat	18.97 \pm 1.12	12.7 \pm 0.61	10	11.3 \pm 0.64	8.49 \pm 0.35	23	9.77 \pm 0.66	7.67 \pm 0.36	12	13.3 \pm 2.85	9.63 \pm 1.57
Mackenzie											
Measured	6.08 \pm 0.94	5.47 \pm 0.35	12	3.51 \pm 0.51	4.57 \pm 0.36	11	3.80 \pm 1.17	4.10 \pm 0.43	4	4.46 \pm 0.81	4.71 \pm 0.40
LOADEST	6.86 \pm 0.15	5.66 \pm 0.04	237	3.64 \pm 0.05	4.61 \pm 0.02	434	5.13 \pm 0.08	4.25 \pm 0.01	280	5.21 \pm 0.93	4.84 \pm 0.42
Landsat	6.01 \pm 0.12	5.6 \pm 0.12	31	4.22 \pm 0.22	4.61 \pm 0.12	25	3.8 \pm 0.29	4.38 \pm 0.16	6	4.68 \pm 0.68	4.86 \pm 0.37
Ob'											
Measured	14.5 \pm 0.58	9.88 \pm 0.37	15	14.0 \pm 0.68	11.2 \pm 0.55	7	9.18 \pm 1.15	9.36 \pm 0.49	4	12.6 \pm 1.69	10.1 \pm 0.54
LOADEST	14.3 \pm 0.05	9.94 \pm 0.01	211	13.0 \pm 0.09	10.3 \pm 0.02	434	12.4 \pm 0.06	10.3 \pm 0.02	280	13.3 \pm 0.56	10.2 \pm 0.12
Landsat	14.2 \pm 0.11	10.1 \pm 0.06	14	13.9 \pm 0.16	9.93 \pm 0.09	19	13.1 \pm 0.21	9.49 \pm 0.12	14	13.7 \pm 0.33	9.84 \pm 0.18
Yenisey											
Measured	17.4 \pm 0.65	10.2 \pm 0.31	15	6.14 \pm 1.05	5.72 \pm 0.59	6	9.01 \pm 1.17	6.70 \pm 0.72	5	10.9 \pm 3.39	7.52 \pm 1.34
LOADEST	16.8 \pm 0.48	9.72 \pm 0.14	172	8.58 \pm 0.04	6.74 \pm 0.02	434	8.52 \pm 0.05	6.46 \pm 0.03	280	11.3 \pm 2.75	7.64 \pm 1.04
Landsat	14.7 \pm 1.25	10.4 \pm 0.69	7	9.04 \pm 0.26	7.26 \pm 0.14	23	9.34 \pm 0.55	7.43 \pm 0.30	4	11.0 \pm 1.83	8.35 \pm 1.01
Yukon											
Measured	14.2 \pm 1.64	10.5 \pm 0.91	15	5.25 \pm 1.36	4.61 \pm 0.66	8	6.55 \pm 1.70	5.65 \pm 1.12	4	8.66 \pm 2.79	6.92 \pm 1.82
LOADEST	12.6 \pm 0.19	9.28 \pm 0.12	254	6.01 \pm 0.07	5.37 \pm 0.04	434	4.75 \pm 0.06	4.8 \pm 0.08	280	7.78 \pm 2.43	6.48 \pm 1.41
Landsat	12.7 \pm 9.27	9.27 \pm 0.31	10	8.15 \pm 0.54	6.77 \pm 0.3	9	5.70 \pm 0.66	5.42 \pm 0.36	5	8.85 \pm 2.05	7.15 \pm 1.13

derived DOC is significantly different than both measured or LOADEST values. Overall, only in four cases did average seasonal CDOM differ significantly from measured or LOADEST values, while DOC differed significantly in six cases (Welch's t -test, p -value < 0.05). In no instance did CDOM or DOC values for the entire ice-free period differ significantly between methods.

3.5. Validation using 2013–2016 Landsat imagery

In comparing measured a_{375} and DOC from Arctic-GRO to remotely-sensed data from 2013 to 2016, we find that our river-specific models are predictive, with slopes close to one (Fig. 7). R^2 across all rivers decreased to 0.67 for CDOM and 0.70 for DOC, in comparison to 0.84

for our calibration dataset (Table 2). This decrease in R^2 is partially related to sample size, as we did not use LOADEST to fill in gaps in the Arctic-GRO database. Removing outliers from the Ob' River does not change R^2 greatly, increasing to 0.71, but the slope decreases from 1.31 to 0.83. The poor performance in predicting DOC based on remote sensing data in the Ob' may be related to shifts in DOM quality. $SUVA_{254}$, for instance was 2.85 and 2.87 $L \text{ mg C}^{-1} \text{ m}^{-1}$ in outliers from 2014 in the Arctic-GRO dataset, but ranged from 2.49 to 4.2 $L \text{ mg C}^{-1} \text{ m}^{-1}$ during the ice-free season when all years are included. There is no apparent relationship to month, season, or discharge during ice-free conditions. Therefore, we do not have confidence in using remotely-sensed CDOM as a proxy for DOC in the Ob' River.

This approach provides an entirely independent check on model

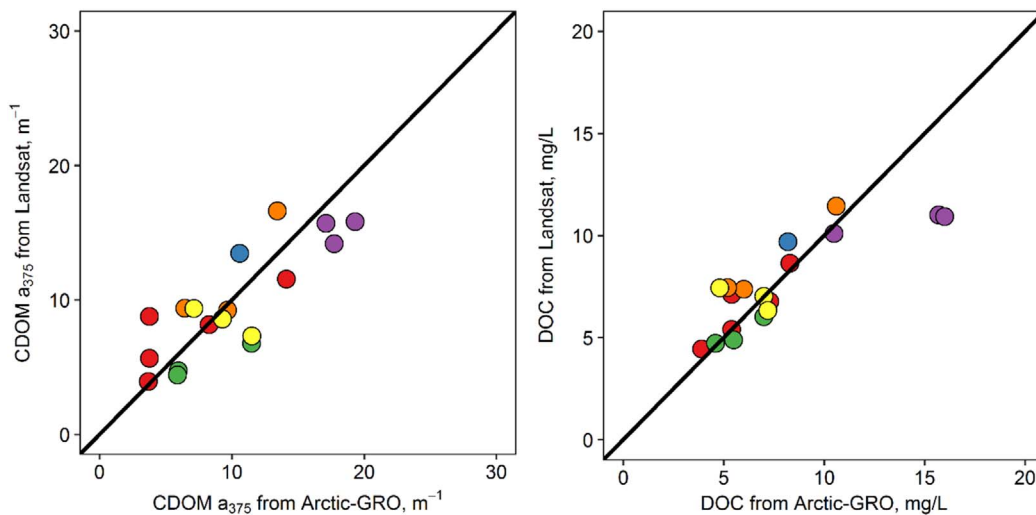


Fig. 7. Comparison of measured Arctic-GRO samples from 2014 to 2016, and 2013 from the Mackenzie River, to CDOM and DOC estimated from Landsat using river-specific algorithms in Table 3. For CDOM, Landsat-estimate = $0.98 \cdot \text{Arctic-GRO} + 0.51$ ($R^2 = 0.67$, $n = 18$, RMSE = 2.68 m^{-1}). For DOC, Landsat-estimate = $1.31 \cdot \text{Arctic-GRO} - 2.25$ ($R^2 = 0.70$, $n = 18$, RMSE = 1.98 mg/L).

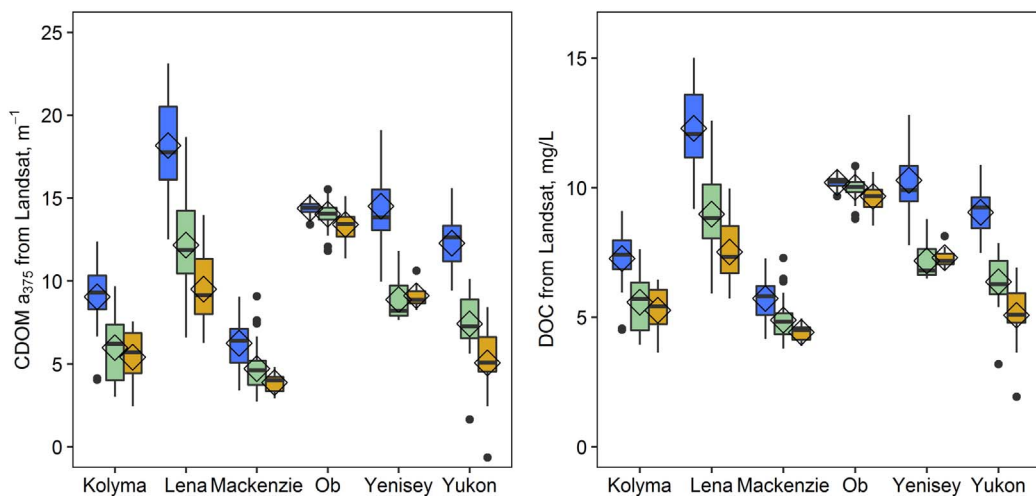


Fig. 8. Seasonal variation in DOM from remote sensing from 2000 to 2013. Boxes are 25th to 75th percentile. Whiskers are 1.5* interquartile range. Lines through boxes are median, diamonds are mean. Points are outliers. Blue = Freshet (May–June), Green = Summer (July–August), Yellow = Fall (September–October). (For interpretation of the references to colour in this figure legend, the reader is referred to the web version of this article.)

performance, as previous Arctic-GRO values were used to model LOADEST and calibrate our remote sensing data. The decrease in R^2 may be partially attributable to error generated by LOADEST in our calibration data. Additionally, there is a potential that using both Landsat 7 and Landsat 8 to generate Fig. 8 could result in biases. However, there was no significant difference between the two sensors (ANOVA, $p = 0.72$). This cross-comparison matches well with previous findings that the two different Landsat platforms are compatible under some conditions (Olmanson et al., 2016).

3.6. DOM during the ice-free season from Landsat data

All rivers display clear seasonal variation during the ice-free period, with the exception of the Ob' River (Fig. 8). The Lena River varies the most, with average DOC concentration of 12.3 mg/L C during spring and 7.5 mg/L C in the fall. The Lena is also the only river where fall and summer DOM differ significantly. In the Kolyma, Mackenzie, Yenisey, and Yukon rivers, spring DOM always substantially exceeds summer and fall. Although not always statistically significant, DOM consistently decreases from spring to summer, and again through fall across all rivers. These relationships hold true for CDOM and DOC. The seasonal signal in these results is strongly linked to discharge. Rivers with tight coupling between discharge and CDOM, such as the Lena and Yenisey, show more robust LOADEST modeling, and a greater variability in DOM across seasons. CDOM in the Mackenzie and Ob' rivers, in contrast, cannot be modeled as successfully using LOADEST, and show the least

variation across the ice-free season. The lowest values in each season come from the Mackenzie River, which also has the lowest average a_{375} of 5.14 m^{-1} . Although the Ob' shows little variation across seasons, it does have the highest average a_{375} and DOC concentration in summer and fall (Fig. 8).

4. Discussion

Remote sensing of CDOM in inland and coastal waters with complex optical properties remains a challenging exercise, particularly at high latitudes where high seasonality, limited datasets, frequent clouds and ice cover, and high solar angles conspire to limit the applicability of satellites. Atmospheric conditions, such as haze, aerosols, and humidity, obscure the low water-leaving radiances of inland waters (Gordon and Wang, 1994; Kutser et al., 2015), necessitating atmospheric correction when retrieving optical properties of complex waters.

Indeed, of the remote sensing signal from a given lake pixel only $\sim 10\%$ is likely attributable to water-leaving radiance, with the remainder a product of atmospheric effects and water surface characteristics such as sun glint or wave action (Dörnhöfer and Oppelt, 2016). This sensitivity to characteristics such as haze, aerosols, and humidity, necessitates reliable atmospheric correction, particularly when using multi-spectral sensors with relatively low radiometric sensitivity like Landsat 5 TM and 7 ETM+ (Lobo et al., 2015; Palmer et al., 2015). Despite these limitations, we were able to build remote sensing

models to estimate CDOM absorption for the major Arctic rivers using the USGS LEDAPS product within GEE. The use of GEE expedited analyses, and showed that automated, cloud-based image processing can produce high quality CDOM datasets. This remote sensing approach more than doubles the number of ice-free observations of CDOM and DOC per river of those available from field measurements from 2000 to 2013, filling in gap years in the measured data set (Fig. 2) and supplementing the bi-monthly Arctic-GRO sampling. The increased observations are generally concentrated in the summer and fall, when hydrological conditions are somewhat more stable. However, permafrost thaw and active layer depths are most extensive during late summer and early fall (Khosh et al., 2017; Zhang et al., 1997). Given the potential late-season interactions between rivers and permafrost in a warming climate (Neff et al., 2006; Striegl et al., 2005; Vonk et al., 2015), this remote sensing approach may be particularly useful for monitoring late-season changes in DOM.

4.1. Comparing measured, LOADEST-derived, and Landsat-derived DOM

CDOM absorption in Arctic rivers can change rapidly over the course of the ice-free season (Mann et al., 2016; Finlay et al., 2006; Peterson et al., 1986). The targeted sampling of PARTNERS was originally designed to address this seasonality, with a particular emphasis on the spring freshet (McClelland et al., 2008; Raymond et al., 2007). More recently (2012 – present), Arctic-GRO switched to a bi-monthly sampling program that alternates between years to generate complete monthly coverage over two-year cycles. While this has improved overall annual coverage, it has resulted in less sampling during the spring. CDOM estimates derived from remote sensing have the potential to make up for this loss of spring coverage. Indeed our Landsat data skew towards the spring: there are more scenes included in our analyses from May–June than September–October owing to the vagaries of cloud cover and the timing of satellite overpasses (Table 2). However, within spring freshet, our remote sensing approach cannot target peak flow conditions as closely as field programs can. For instance, only 10% of the Landsat scenes observe May through the first week of June, when discharge peaks on most rivers (Fig. 2). Early freshet samples contribute 22% of the Arctic-GRO dataset during the ice-free season. Thus, particularly on the Kolyma and Lena rivers, average CDOM absorption and DOC concentrations estimated from remote sensing in spring tend to be lower than from field-based measurements. LOADEST lacks this bias towards peak flow, and Landsat results match LOADEST more closely, with only DOC from the Kolyma significantly different between the two methods in spring (Table 4). The significant differences between Landsat and other methods in the Ob' and Yukon rivers cannot be easily attributed to such seasonal biases, however. CDOM absorption and DOC concentrations in the Ob' do not vary seasonally or annually as much as other rivers considered here; thus, despite the statistical significance, mean seasonal DOC in the Ob' never differs between methods > 1.25 mg/L. In the Yukon, suspended sediments may be artificially inflating Landsat-derived estimates of CDOM in summer or fall. Despite these anomalies, average Landsat-derived CDOM and DOC for most seasons and across the total ice-free period for all rivers consistently reflect both measured and LOADEST datasets.

Our Landsat-based approach increases the frequency of observations in summer (Table 4), during which time permafrost thaw and thermokarst activity are likely to be highest (Liu et al., 2015; Osterkamp et al., 2000). While only a portion of DOM in large rivers originates in aged permafrost soils (Raymond et al., 2007; Spencer et al., 2015), a distinct seasonal signal indicating that permafrost carbon can be a significant source of riverine DOM during the summer and fall (Feng et al., 2017; Neff et al., 2006). Late season changes in concentration or composition of organic matter could be reflective of deepening hydrological flowpaths or the mobilization of permafrost carbon (Pokrovsky et al., 2015; Striegl et al., 2005). With a nearly three-fold increase in summer CDOM estimates using Landsat, we may be able to observe

more subtle climate-induced shifts in riverine CDOM.

Furthermore, the launch of the paired Sentinel-2 A&B satellites, with ongoing data collection by Landsat 8 OLI, will provide an increased frequency of satellite overpasses, particularly at high latitudes owing to their polar orbiting pathways. These newer satellites were intended to provide continuity to historical satellite records while improving signal-to-noise ratios and adding specialized bands (Loveland and Irons, 2016; Mishra et al., 2016). Recent research has shown that Landsat 8 can be used for improved estimates of CDOM in inland waters (Brezonik et al., 2015; Herrault et al., 2016; Olmanson et al., 2016), as its radiometric performance has been increased from 8 bit data in earlier Landsat sensors to 12 bit. Initial work on modeled Sentinel-2 results indicate improved sensitivity to water quality parameters, as well (Kutser et al., 2016; Manzo et al., 2015). Future work will be necessary to link Sentinel-2 and Landsat 8 to historical imagery for CDOM time series, although there is preliminary evidence of compatibility (Olmanson et al., 2016), and our own data (Fig. 7, Section 3.5).

4.2. Watershed characteristics as controls on remote sensing of CDOM

The six Arctic-GRO rivers represent 67% of the Arctic Ocean watershed (Holmes et al., 2012), and vary widely in watershed characteristics that influence riverine organic matter and our ability to remotely sense CDOM. While our overall ability to estimate CDOM and DOC from Landsat imagery is comparable to other studies on remote sensing of inland waters (Olmanson et al., 2016), the differences in river-specific models may be driven by hydrological and biogeochemical characteristics that vary by watershed. CDOM remote sensing models are most robust when measured and LOADEST modeled values vary widely across seasons, with highest absorption found during the spring freshet. Ranges of CDOM absorption from LOADEST are widest in the Yenisey (Table 4), which also features the strongest relationship between remotely sensed CDOM and calibration data (Table 3) and relatively low concentrations of TSS that may also influence optical properties. The Mackenzie and Ob' rivers vary relatively little in CDOM throughout the ice-free season compared to other rivers (Table 4). In consequence of the relatively stable CDOM, the regressions lack the power to explain the variance seen in these rivers. Despite this limitation, RMSE for the Mackenzie and Ob' are comparable to other rivers (Table 3), and group with other rivers when calibration data and remote sensing estimates are plotted together (Fig. 4). Additional error in the Mackenzie River may originate from the use of frozen CDOM samples. Cryopreservation effects can be large within the Mackenzie River, particularly when CDOM absorption is low (Griffin, 2016).

Many Arctic rivers are hydrologically “flashy” during the spring freshet, with a peak in discharge followed by lower flow during the summer (Fig. 2). DOM concentrations correlate positively with discharge, and shift in source and composition across the hydrograph (Neff et al., 2006; Raymond et al., 2007; Spencer and Aiken, 2009; Wickland et al., 2007). However, discharge fails to explain CDOM absorption in the Mackenzie or Ob' as it does in the other rivers. Both the Mackenzie and Ob' have a less distinctive peak in spring discharge (Fig. 2), and measured a_{375} and DOC change less over the course of the ice-free season than in other large Arctic rivers (Fig. 8). Several watershed features may contribute to these characteristics. The Mackenzie contains Great Slave Lake, Great Bear Lake, and the inland Peace-Athabasca delta. These large lake systems mediate seasonal discharge, and place a strong lake storage effect upon the Mackenzie River (Woo and Thorne, 2003). The extensive non-permafrost peatlands in the Ob' watershed retain large amounts of water, and may have a similar effect on attenuating streamflow as the extensive lakes found in the Mackenzie (Smith et al., 2012).

Sediment loads, which influence the overall reflectance of natural waters across the visible spectrum (Lymburner et al., 2016), also contribute to river-specific relationships between remote sensing data and CDOM concentrations. Concentrations of total suspended solids (TSS)

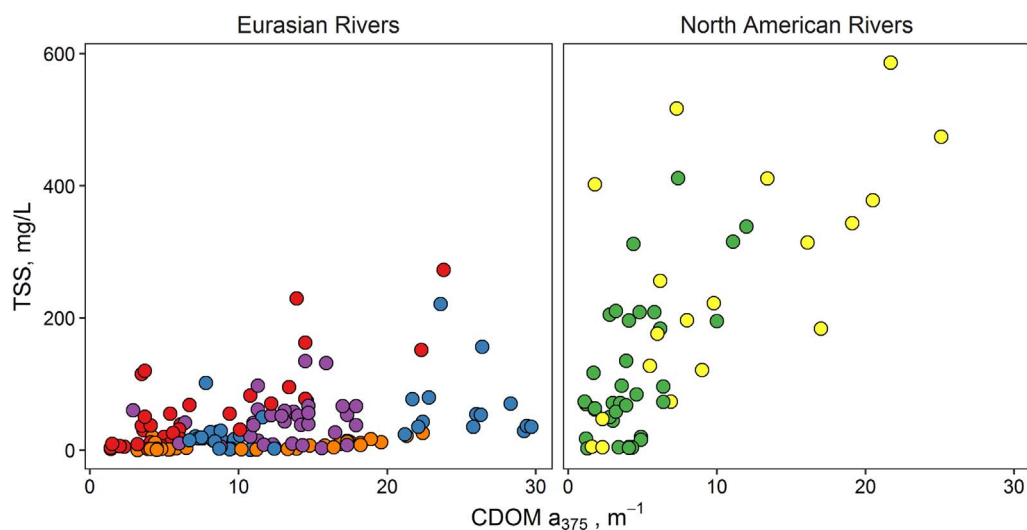


Fig. 9. CDOM a_{375} (m^{-1}) versus TSS (mg/L) for the Eurasian (left) and North American (right) rivers. Red = Kolyma, Green = Mackenzie, Orange = Yenisey, Blue = Lena, Purple = Ob', Yellow = Yukon. (For interpretation of the references to colour in this figure legend, the reader is referred to the web version of this article.)

generally increase with river discharge and are highest during the spring freshet (Holmes et al., 2002). However, TSS concentrations vary widely among the major Arctic rivers (Fig. 9). TSS concentrations peak at ~ 30 mg/L in the Yenisey River, whereas concentrations exceed 400 mg/L in the Yukon and Mackenzie. TSS concentrations in the other rivers are intermediate within this range. High TSS concentrations do not necessarily interfere with our ability to estimate CDOM, but correlations between CDOM and TSS (Fig. 9; Table S1) become an increasingly important consideration as sediment contributions go up. In the Mackenzie, TSS concentrations increase more rapidly relative to increases in CDOM (slope = 23.43) than any other river (Table S1), indicating that the remote sensing signal may be more responsive to changes in TSS than CDOM. The Yukon, in contrast, has some of the highest CDOM levels in our dataset, and relative increases in TSS on par with the Kolyma River despite high sediment concentrations. Few studies have addressed remote sensing of both CDOM and sediments in waters where both are high, and teasing apart the two signals can be difficult (Pavelsky and Smith, 2009). Algorithms relating remotely sensed parameters to CDOM in high sediment waters can be applied confidently within the calibration timeframe, but potential changes in CDOM-sediment relationships may confound interpretation of remote sensing data outside the calibration timeframe.

The results presented in Table 3 are purely empirical, and only the Kolyma and Yenisey rivers share common band combinations. However, these differences may further inform the theoretical underpinnings of using satellite remote sensing to monitor CDOM, for which we still have limited understanding (Brezonik et al., 2015). Green and red bands appeared most frequently in our models, including a “universal” regression based on all rivers grouped together (Table 3). The ratio of green to red reflectance is commonly used in other empirical approaches to remote sensing of CDOM in complex waters (Brezonik et al., 2015; Ficek et al., 2011; Kutser et al., 2005; Menken et al., 2006). Although CDOM absorption decreases exponentially with increasing wavelength, the functional light-paths of inland waters measured from space are much longer than lab techniques. Thus, there is a greater CDOM signal at longer wavelengths than might otherwise be measured through laboratory techniques. This may explain partially why longer wavelengths (e.g., Landsat TM and ETM+ bands 2 and 3) can still strongly relate to CDOM absorption in UV or blue wavelengths (350–440 nm). Furthermore, because atmospheric effects tend to be largest in the blue region (400–500 nm), reflectance from green and red wavelengths may be preferred in regression-based approaches (Kutser et al., 2005).

Although it has been suggested that reflectance near 670 nm linked to a chlorophyll-*a* correction in remote sensing of CDOM studies, the low chlorophyll concentrations in many Arctic rivers indicate this may not be the sole explanation for the inclusion of these longer wavelengths. Reflectance in NIR wavelengths appears in empirical models from the Lena, Mackenzie, and Yukon rivers. NIR reflectance has long been used to estimate TSS or suspended sediment concentrations (SSC) in inland and coastal waters, with some indication that models may be transferrable between systems (Long and Pavelsky, 2013; Novo et al., 1989; Quibell, 1991). As discussed above, these rivers may be influenced by TSS to varying degrees, given relative TSS concentrations and CDOM levels.

The high sediment loads in the Mackenzie River may also influence our ability to spatially extrapolate models based upon temporal variability (Figs. 5 and 6). The Mackenzie is the single largest exporter of sediment to the Arctic Ocean (Holmes et al., 2002), and surface TSS concentrations can exceed 1000 mg/L in the delta during spring freshet (Griffin and Vonk, unpublished data). In early June, the Mackenzie floods lakes and inundates wetlands throughout the delta (Marsh and Hey, 1989). Particulate matter may settle out or become re-suspended, depending on water levels and velocities (Emmerton et al., 2007), while dissolved constituents may remain more stable, thus decoupling TSS and CDOM. The inability of our remote sensing approach to accurately estimate CDOM at delta sites in the Mackenzie support the idea that the model for this river may be more strongly influenced by variability in suspended sediment. Alternatively, Our Mackenzie model may not adequately represent CDOM conditions in the delta because they are far outside of our calibration range: while a_{440} in the Mackenzie delta can exceed $20 m^{-1}$, the calibration data only ranges 2.16–11.43 m^{-1} . However, CDOM from tributaries in the Kolyma watershed, and along a river continuum, are estimated with better accuracy than any of the Mackenzie delta samples. Without a larger dataset, extrapolating the Kolyma remote sensing model to include major tributaries must be done conservatively. However, this dataset adds to our confidence in mapping CDOM throughout the lower main stem of the Kolyma (Griffin et al., 2011), and suggests that these models can be used to assess spatial variability within some river systems. The ability to spatially extrapolate from a limited number of ground-truthing sites remains a key advantage of remote sensing approaches, but needs further validation before it can be applied confidently in Arctic rivers. In addition, these methods should not yet be applied to other nearby rivers, without further validation. Previous studies have used bio-optical models to relate remote sensing signal to individual inherent optical properties,

e.g. CDOM, and backscatter of non-algal particles. Such studies have even been conducted along the Mackenzie River shelf (Belanger et al., 2008; Doxaran et al., 2012). These bio-optical models offer the ability to differentiate between each optical property, but must be measured at each location. Suspended sediment, for instance, can be optically different based on particle size, shape, and mineralogy (Novo et al., 1989). Thus, in situ backscatter and reflectance measurements should be used to help calibrate bio-optical models, which have not yet been performed for most of the Arctic-GRO river systems. Additionally, multi-decadal time series analyses may allow researchers to find climate-driven changes in DOM fluxes or concentrations, associated with either anthropogenic climate change (Tank et al., 2016; Toohey et al., 2016) or large-scale climate patterns (Fichot et al., 2013). However, these datasets should be interpreted cautiously given the uncertainties inherent in using older generation satellite platforms such as Landsat TM and ETM+. Such uncertainties include both the complex optical relationships between TSS and CDOM, and the possibility of changing CDOM sources leading to a shift in DOC-CDOM relationships on decadal timescales.

4.3. Remotely sensed CDOM as a proxy for other DOM characteristics

While strong relationships between a_{375} and DOC concentrations have been leveraged in a variety of recent studies, it is noteworthy that DOC and dissolved organic nitrogen (DON) are also strongly correlated in Arctic rivers (Frey et al., 2007; Holmes et al., 2012; McClelland et al., 2014). Riverine DON may be particularly important to coastal ecosystems, as it greatly exceeds dissolved inorganic nitrogen (DIN) in these six Arctic rivers (Le Fouest et al., 2013; Tank et al., 2012). Both bacterial and photochemical remineralization of DON could contribute to production in Arctic coastal waters (Bélanger et al., 2006; Le Fouest et al., 2013). Although beyond the scope of this study, it might be possible to use relationships between CDOM, DOC, and DON to calculate satellite-derived estimates of DON concentrations.

Remotely sensed CDOM may be a useful proxy for other DOM characteristics as well. Stubbins et al. (2015) proposed using absorption at 412 nm to predict dissolved black carbon (DBC) from the Arctic-GRO rivers, with $R^2 > 0.97$. The aromatic compounds that form DBC strongly absorb light, explaining a mechanistic link between DBC and CDOM. Additionally, Walker et al. (2013) showed that lignin phenol concentrations in the Kolyma, Lena, and Yenisey rivers could be estimated from a_{350} . Lignin phenols, derived from plant matter, have been widely used as terrestrial biomarkers in aquatic and marine systems. These results have more recently been corroborated for all of the Arctic-GRO rivers (Mann et al., 2016). The above methods rely upon absorption at a single wavelength in the UV-A (315–400 nm) or visible spectrum (400–800 nm) as a proxy for different types of aromatic compounds, and are based upon the same rivers analyzed in this application. Although there are some differences in spectral slope within the Arctic-GRO dataset (Walker et al., 2013), a_{375} correlates strongly with a_{350} ($R^2 = 0.996$) and a_{412} ($R^2 = 0.978$). Thus, our remote sensing estimates of a_{375} could potentially be used to derive concentrations of DBC and lignins through these proxies established elsewhere. The Arctic-GRO database provides a rare opportunity to explore the empirical relationships between CDOM and labor-intensive molecular measurements of organic matter. Extrapolating such relationships to remote sensing of Arctic rivers should be performed cautiously.

5. Conclusions

Estimation of CDOM in the major Arctic rivers from Landsat data provides a new tool to synoptically monitor river biogeochemistry on a Pan-Arctic scale. We built river-specific empirical models between satellite reflectance and LOADEST-modeled CDOM over six Arctic rivers, using 424 separate observations from 2000 to 2013. In the Kolyma, Lena, Yenisey, and Yukon rivers, this regression-based approach

predicted CDOM with R^2 values of 0.67–0.84, and RMSE values of 1.17–2.96 m^{-1} . Relationships between CDOM and remotely sensed parameters were weaker in the Mackenzie and Ob' rivers (R^2 of 0.53 and 0.33, RMSE of 1.45 m^{-1} and 1.21 m^{-1} , respectively), likely owing to a relative lack in inherent CDOM variability for the regression models to explain. Sediment may also have been a confounding factor, particularly in the Mackenzie River.

The approach we have described here addresses two common issues in remote sensing of inland waters. First, collecting field data that corresponds with clear-sky satellite imagery – particularly in remote regions like the Arctic – has long been a challenge to the development of empirical relationships between CDOM and remotely sensed surface reflectance. By using LOADEST, we were able to overcome this limitation and create a year-round daily dataset. Although using this approach did introduce some uncertainty, both the LOADEST and the subsequent Landsat-derived CDOM absorption matched well with seasonally-averaged data from measured Arctic-GRO data. Secondly, using Google Earth Engine (GEE) greatly improved the efficiency of analyses, by allowing for the entire Landsat record at any given location to be filtered based on cloud cover, Julian day, year, and other relevant parameters. The capabilities of GEE have been expanding rapidly, as new datasets and analytical methods are added, making this platform an important new tool in remote sensing fields. The remote sensing equations we have developed may be applied to both historical and future Landsat imagery, with the caveat that shifts in CDOM quality and/or TSS-CDOM correlations could alter river-specific relationships between CDOM and remotely sensed parameters. In rivers with high CDOM and low TSS, such as the Yenisey, it may be possible to automate CDOM remote sensing, especially through the use of the USGS Surface Reflectance Product (Schmidt et al., 2013) and Google Earth Engine. Although USGS Surface Reflectance methods were not originally intended to be used for remote sensing of water quality parameters, our results show that this product is effective for such applications.

Satellite-derived CDOM will allow assessment of climate change impacts on riverine DOM fluxes to the Arctic Ocean, and extend time series to the 1980s in some rivers. Future research based upon the approach described here will explore climate-driven trends in CDOM concentration and export. By applying the remote sensing algorithms developed in this study to historical imagery, we can produce time series of CDOM absorption and fluxes that are independent of changes in discharge-constituent relationships. There is potential to also observe shifts in DOC, although such estimates depend on assuming the correlation between CDOM and DOC does not change through time. As remote sensing of complex waters improves with new sensors, these riverine endmembers can complement other efforts to trace terrestrial DOM into the Arctic Ocean with ocean-colour remote sensing (Fichot et al., 2013). The remotely-sensed data products may be further used to monitor CDOM across watersheds or trace pulses of CDOM throughout a river network (Herrault et al., 2016), although additional work needs to be conducted to validate such spatial extrapolations. New sensors, such as Landsat 8 and Sentinel-2, offer improved sensitivity for estimating CDOM owing to better band placement and increased radiometric resolution, as well as increased frequency of observations throughout the ice-free season. These new sensors, particularly Sentinel-2 with an improved band placement for remote sensing of water quality, could potentially be used to develop more universal, semi-analytical algorithms that also retrieve TSS and chlorophyll. Furthermore, riverine CDOM has been strongly tied to many terrestrial biomarkers, such as lignin, humics, and molecular weight, and thus may be useful for remote estimations of important terrestrial-aquatic linkages. Once established, Landsat-based approximations of CDOM provide an important supplement to field and laboratory intensive efforts to monitor the rapidly changing Arctic carbon cycle.

Acknowledgements

We thank the following for support with field sampling, logistics and laboratory analyses: Sam Berman, Ekaterina Bulygina, Patty Garlough, Suzanne Tank, Elise van Winden, Jorien Vonk, and Nikita Zimov. This material is based upon work supported by the NSF Graduate Research Fellowship under Grant No. DGE-1610403, the Arctic Great Rivers Observatory (NSF Grant Nos. 0229302, 0732985, 0732821, and 1107774; www.arcticgreatrivers.org), and the Polaris Project II (NSF Grant No. 1044610; www.thepolarisproject.org).

Appendix A. Supplementary data

Supplementary data to this article can be found online at <https://doi.org/10.1016/j.rse.2018.02.060>.

References

- Aagard, K., Carmack, E.C., 1989. The role of sea ice and other fresh water in the Arctic circulation. *J. Geophys. Res.* 94, 14,414–485,498. <http://dx.doi.org/10.1029/JC094iC10p14485>.
- Alling, V., Sanchez-Garcia, L., Porcelli, D., Pugach, S., Vonk, J.E., van Dongen, B., Mörth, C.-M., Anderson, L.G., Sokolov, A., Andersson, P., Humborg, C., Semiletov, I., Gustafsson, Ö., 2010. Nonconservative behavior of dissolved organic carbon across the Laptev and East Siberian seas. *Glob. Biogeochem. Cycles* 24, 1–15. <http://dx.doi.org/10.1029/2010GB003834>.
- Béanger, S., Xie, H., Krotkov, N., Larouche, P., Vincent, W.F., Babin, M., 2006. Photomineralization of terrigenous dissolved organic matter in arctic coastal waters from 1979 to 2003: interannual variability and implications of climate change. *Glob. Biogeochem. Cycles* 20, 1–13. <http://dx.doi.org/10.1029/2006GB02708>.
- Belanger, S., Babin, M., Larouche, P., 2008. An empirical ocean color algorithm for estimating the contribution of chromophoric dissolved organic matter to total light absorption in optically complex waters. *J. Geophys. Res. Oceans* 113, 1–14. <http://dx.doi.org/10.1029/2007JC004436>.
- Belzile, C., Gibson, J.A.E., Vincent, W.F., 2002. Colored dissolved organic matter and dissolved organic carbon exclusion from lake ice: implications for irradiance transmission and carbon cycling. *Limnol. Oceanogr.* 47, 1283–1293. <http://dx.doi.org/10.4319/lo.2002.47.5.1283>.
- Brezonik, P., Menken, K., Bauer, M., 2005. Landsat-based remote sensing of lake water quality characteristics, including chlorophyll and colored dissolved organic matter (CDOM). *Lake Reservoir Manage.* 21, 373–382. <http://dx.doi.org/10.1080/07438140509354442>.
- Brezonik, P.L., Olmanson, L.G., Finlay, J.C., Bauer, M.E., 2015. Factors affecting the measurement of CDOM by remote sensing of optically complex inland waters. *Remote Sens. Environ.* 157, 199–215. <http://dx.doi.org/10.1016/j.rse.2014.04.033>.
- Claverie, M., Vermote, E.F., Franch, B., Masek, J.G., 2015. Remote Sensing of Environment Evaluation of the Landsat-5 TM and Landsat-7 ETM + Surface Reflectance Products. vol. 169. pp. 390–403.
- Cooper, L.W., Benner, R., McClelland, J.W., Peterson, B.J., Holmes, R.M., Raymond, P.A., Hansell, D.A., Grebmeier, J.M., Codispoti, L.A., 2005. Linkages Among Runoff, Dissolved Organic Carbon, and the Stable Oxygen Isotope Composition of Seawater and Other Water Mass Indicators in the Arctic Ocean.
- Dörnhöfer, K., Oppelt, N., 2016. Remote sensing for lake research and monitoring—recent advances. *Ecol. Indic.* 64, 105–122.
- Doxaran, D., Ehn, J., Belanger, S., Matsuoaka, A., Hooker, S., Babin, M., 2012. Optical Characterisation of Suspended Particles in the Mackenzie River Plume (Canadian Arctic Ocean) and Implications for Ocean Colour Remote Sensing. pp. 3213–3229. <http://dx.doi.org/10.5194/bg-9-3213-2012>.
- Elmqvist, M., Semiletov, I., Guo, L., Gustafsson, Ö., 2008. Pan-Arctic patterns in black carbon sources and fluvial discharges deduced from radiocarbon and PAH source apportionment markers in estuarine surface sediments. *Glob. Biogeochem. Cycles* 22, 1–13. <http://dx.doi.org/10.1029/2007GB002994>.
- Emmerton, C.a., Lesack, L.F.W., Marsh, P., 2007. Lake abundance, potential water storage, and habitat distribution in the Mackenzie River Delta, western Canadian Arctic. *Water Resour. Res.* 43, 1–14. <http://dx.doi.org/10.1029/2006WR005139>.
- Emmerton, C.a., Lesack, L.F.W., Vincent, W.F., 2008. Nutrient and organic matter patterns across the Mackenzie River, estuary and shelf during the seasonal recession of sea-ice. *J. Mar. Syst.* 74, 741–755. <http://dx.doi.org/10.1016/j.jmarsys.2007.10.001>.
- Feng, X., Vonk, J.E., Griffin, C., Zimov, N., Montlucón, D.B., Wacker, L., Eglinton, T.I., 2017. 14C variation of dissolved lignin in arctic river systems. *ACS Earth Space Chem.* 0 (null). <https://doi.org/10.1021/acsearthspacechem.7b00055>.
- Ficek, D., Zapadka, T., Dera, J., 2011. Remote sensing reflectance of Pomeranian lakes and the Baltic. *Oceanologia* 53, 959–970. <http://dx.doi.org/10.5697/oc.53-4.959>.
- Fichot, C.G., Kaiser, K., Hooker, S.B., Amon, R.M.W., Babin, M., Béanger, S., Walker, S.A., Benner, R., 2013. Pan-Arctic distributions of continental runoff in the Arctic Ocean. *Sci. Rep.* 3, 1–6. <http://dx.doi.org/10.1038/srep01053>.
- Finlay, J., Neff, J., Zimov, S., Davydova, A., Davydov, S., 2006. Snowmelt dominance of dissolved organic carbon in high-latitude watersheds: implications for characterization and flux of river DOC. *Geophys. Res. Lett.* 33, L10401.
- Frey, K.E., McClelland, J.W., 2009. Impacts of permafrost degradation on arctic river biogeochemistry. *Hydrol. Process.* 23, 169–182. <http://dx.doi.org/10.1002/hyp.7196>.
- Frey, K.E., McClelland, J.W., Holmes, R.M., Smith, L.C., 2007. Impacts of climate warming and permafrost thaw on the riverine transport of nitrogen and phosphorus to the Kara Sea. *J. Geophys. Res.* 112, 1–10. <http://dx.doi.org/10.1029/2006JG000369>.
- Frey, K.E., Sobczak, W.V., Mann, P.J., Holmes, R.M., 2016. Optical properties and bioavailability of dissolved organic matter along a flow-path continuum from soil pore waters to the Kolyma River, Siberia. *Biogeosciences* 12, 12321–12347. <http://dx.doi.org/10.5194/bg-12-12321-2015>.
- Gordon, H.R., Wang, M., 1994. Retrieval of water-leaving radiance and aerosol optical thickness over the oceans with SeaWiFS: a preliminary algorithm. *Appl. Opt.* 33, 443–452. <http://dx.doi.org/10.1364/AO.33.00443>.
- Gorelick, N., Hancher, M., Dixon, M., Ilyushchenko, S., Thau, D., Moore, R., 2017. Remote sensing of environment Google Earth Engine: planetary-scale geospatial analysis for everyone. *Remote Sens. Environ.* <http://dx.doi.org/10.1016/j.rse.2017.06.031>.
- Griffin, C.G., 2016. Dissolved Organic Matter in Major Rivers across the Pan-Arctic from Remote Sensing.
- Griffin, C.G., Frey, K.E., Rogan, J., Holmes, R.M., 2011. Spatial and interannual variability of dissolved organic matter in the Kolyma River, East Siberia, observed using satellite imagery. *J. Geophys. Res. Biogeosci.* 116, 1–12. <http://dx.doi.org/10.1029/2010JG001634>.
- Guo, L., Cai, Y., Belzile, C., Macdonald, R.W., 2012. Sources and export fluxes of inorganic and organic carbon and nutrient species from the seasonally ice-covered Yukon River. *Biogeochemistry* 107, 187–206. <http://dx.doi.org/10.1007/s10533-010-9545-z>.
- Gustafsson, Ö., Van Dongen, B.E., Vonk, J.E., Dudarev, O.V., Semiletov, I.P., 2011. Widespread release of old carbon across the Siberian Arctic echoed by its large rivers. *Biogeosciences* 8, 1737–1743. <http://dx.doi.org/10.5194/bg-8-1737-2011>.
- Hansen, M.C., Potapov, P.V., Moore, R., Hancher, M., Turubanova, S.A., Tyukavina, A., 2013. High-resolution global maps of 21st-century forest cover change. *Science* 80 (342), 850–853. <http://dx.doi.org/10.1126/science.1244693>.
- Herrault, P.A., Gandois, L., Gascois, S., Tananaev, N., Le Dantec, T., Teisserenc, R., 2016. Using high spatio-temporal optical remote sensing to monitor dissolved organic carbon in the Arctic river Yenisei. *Remote Sens.* 8. <http://dx.doi.org/10.3390/rs8100803>.
- Holmes, R.M., McClelland, J.W., Peterson, B.J., Shiklomanov, I.A., Zhulidov, A.V., Gordeev, V.V., Bobrovitskaya, N.N., 2002. A circumpolar perspective on fluvial sediment flux to the Arctic ocean. *Glob. Biogeochem. Cycles* 16, 14–45. <http://dx.doi.org/10.1029/2001GB001849>.
- Holmes, R.M., McClelland, J.W., Peterson, B.J., Tank, S.E., Bulygina, E., Eglinton, T.I., Gordeev, V.V., Gurtovaya, T.Y., Raymond, P.A., Repeta, D.J., Staples, R., Striegl, R.G., Zhulidov, A.V., Zimov, S.A., 2012. Seasonal and annual fluxes of nutrients and organic matter from large rivers to the Arctic Ocean and surrounding seas. *Estuar. Coasts* 35, 369–382. <http://dx.doi.org/10.1007/s12237-011-9386-6>.
- Hu, C.M., Muller-Karger, F.E., Zepp, R.G., 2002. Absorbance, absorption coefficient, and apparent quantum yield: a comment on common ambiguity in the use of these optical concepts. *Limnol. Oceanogr.* 47, 1261–1267. <http://dx.doi.org/10.4319/lo.2002.47.4.1261>.
- Huntington, J., McGwire, K., Morton, C., Snyder, K., Peterson, S., Erickson, T., Niswonger, R., Carroll, R., Smith, G., Allen, R., 2016. Assessing the role of climate and resource management on groundwater dependent ecosystem changes in arid environments with the Landsat archive. *Remote Sens. Environ.* 185, 186–197. <http://dx.doi.org/10.1016/j.rse.2016.07.004>.
- Joshi, I., Sa, E.J.D., 2015. Seasonal Variation of Colored Dissolved Organic Matter in Barataria Bay, Louisiana, Using Combined Landsat and Field Data. pp. 12478–12502. <http://dx.doi.org/10.3390/rs70912478>.
- Kallio, K., Attila, J., Härmä, P., Koponen, S., Pulliainen, J., Hyttiäinen, U.-M., Pyhälähti, T., 2008. Landsat ETM+ images in the estimation of seasonal Lake water quality in Boreal River basins. *Environ. Manag.* 42, 511–522. <http://dx.doi.org/10.1007/s00267-008-9146-y>.
- Kaufman, Y.J., Wald, A.E., Remer, L.A., Gao, B.-C., Li, R.-R., Flynn, L., 1997. The MODIS 2.1um channel-correlation with visible reflectance for use in remote sensing of aerosol. *IEEE Trans. Geosci. Remote Sens.* 35, 1286–1298. <http://dx.doi.org/10.1109/36.628795>.
- Khosh, M.S., McClelland, J.W., Jacobson, A.D., Douglas, T.A., Barker, A.J., Lehn, G.O., 2017. Seasonality of dissolved nitrogen from spring melt to fall freezeup in Alaskan Arctic tundra and mountain streams. *J. Geophys. Res. Biogeosci.* 122, 1718–1737. <http://dx.doi.org/10.1002/2016JG003377>.
- Kutser, T., 2012. The possibility of using the Landsat image archive for monitoring long time trends in coloured dissolved organic matter concentration in lake waters. *Remote Sens. Environ.* 123, 334–338. <http://dx.doi.org/10.1016/j.rse.2012.04.004>.
- Kutser, T., Pierson, D.C., Kallio, K.Y., Reinart, A., Sobek, S., 2005. Mapping lake CDOM by satellite remote sensing. *Remote Sens. Environ.* 94, 535–540. <http://dx.doi.org/10.1016/j.rse.2004.11.009>.
- Kutser, T., Verpoorter, C., Paavel, B., Tranvik, L.J., 2015. Estimating lake carbon fractions from remote sensing data. *Remote Sens. Environ.* 157, 138–146. <http://dx.doi.org/10.1016/j.rse.2014.05.020>.
- Kutser, T., Paavel, B., Verpoorter, C., Ligi, M., Soomets, T., Toming, K., Casal, G., 2016. Remote sensing of black lakes and using 810 nm reflectance peak for retrieving water quality parameters of optically complex waters. *Remote Sens.* 8. <http://dx.doi.org/10.3390/rs8060497>.
- Larouche, J.R., Abbott, B.W., Bowden, W.B., Jones, J.B., 2015. The role of watershed characteristics, permafrost thaw, and wildfire on dissolved organic carbon biodegradability and water chemistry in Arctic headwater streams. *Biogeosciences* 12, 4221–4233. <http://dx.doi.org/10.5194/bg-12-4221-2015>.
- Le Fouest, V., Babin, M., Tremblay, J.E., 2013. The fate of riverine nutrients on Arctic

- shelves. *Biogeosciences* 10, 3661–3677. <http://dx.doi.org/10.5194/bg-10-3661-2013>.
- Liu, L., Schaefer, K.M., Chen, A.C., Gusmeroli, A., Zebker, H.A., Zhang, T., 2015. Journal of Geophysical Research: Earth Surface Remote Sensing Measurements of Thermokarst Subsidence Using InSAR 1935–1948. <http://dx.doi.org/10.1002/2015JF003599>. (Received).
- Lobo, F.L., Costa, M.P.F., Novo, E.M.L.M., 2015. Time-series analysis of Landsat-MSS/TM/OLI images over Amazonian waters impacted by gold mining activities. *Remote Sens. Environ.* 157, 170–184. <http://dx.doi.org/10.1016/j.rse.2014.04.030>.
- Long, C.M., Pavelsky, T.M., 2013. Remote sensing of suspended sediment concentration and hydrologic connectivity in a complex wetland environment. *Remote Sens. Environ.* 129, 197–209. <http://dx.doi.org/10.1016/j.rse.2012.10.019>.
- Loveland, T.R., Irons, J.R., 2016. Landsat 8: the plans, the reality, and the legacy. *Remote Sens. Environ.* 185, 1–6. <http://dx.doi.org/10.1016/j.rse.2016.07.033>.
- Lymburner, L., Botha, E., Hestir, E., Anstee, J., Sagar, S., Dekker, A., Malthus, T., 2016. Landsat 8: providing continuity and increased precision for measuring multi-decadal time series of total suspended matter. *Remote Sens. Environ.* 185, 108–118. <http://dx.doi.org/10.1016/j.rse.2016.04.011>.
- Maiersperger, T.K., Scaramuzza, P.L., Leigh, L., Shrestha, S., Gallo, K.P., Jenkerson, C.B., Dwyer, J.L., 2013. Characterizing LEDAPS surface reflectance products by comparisons with AERONET, field spectrometer, and MODIS data. *Remote Sens. Environ.* 136, 1–13. <http://dx.doi.org/10.1016/j.rse.2013.04.007>.
- Manizza, M., Follows, M.J., Dutkiewicz, S., Menemenlis, D., McClelland, J.W., Hill, C.N., Peterson, B.J., Key, R.M., 2011. A model of the Arctic Ocean carbon cycle. *Carbon N. Y.* 116, 1–19. <http://dx.doi.org/10.1029/2011JC006998>.
- Mann, P.J., Davydova, A., Zimov, N.S., Spencer, R., Davydov, S., Bulygina, E., Zimov, S.A., Holmes, R.M., 2012. Controls on the composition and lability of dissolved organic matter in Siberia's Kolyma River basin. *J. Geophys. Res.* 117, 1–15. <http://dx.doi.org/10.1029/2011JG001798>.
- Mann, P.J., Spencer, R.G.M., Dinga, B.J., Poulsen, J.R., Hernes, P.J., Fiske, G., Salter, M.E., Wang, Z.A., Hoering, K.A., Six, J., Holmes, R.M., 2014. The biogeochemistry of carbon across a gradient of streams and rivers within the Congo Basin. *J. Geophys. Res. Biogeosci.* 119. <http://dx.doi.org/10.1002/2013JG002442>.
- Mann, P.J., Eglinton, T.I., McIntyre, C.P., Zimov, N., Davydova, A., Vonk, J.E., Holmes, R.M., Spencer, R.G.M., 2015. Utilization of ancient permafrost carbon in headwaters of Arctic fluvial networks. *Nat. Commun.* 6, 1–7. <http://dx.doi.org/10.1038/ncomms8856>.
- Mann, P.J., Spencer, R.G.M., Hernes, P.J., Six, J., Aiken, G.R., Tank, S.E., McClelland, J.W., Butler, K.D., Dyda, R.Y., Holmes, R.M., 2016. Pan-Arctic trends in terrestrial dissolved organic matter from optical measurements. *Front. Earth Sci.* 4, 1–18. <http://dx.doi.org/10.3389/feart.2016.00025>.
- Manzo, C., Bresciani, M., Giardino, C., Braga, F., Bassani, C., 2015. Sensitivity analysis of a bio-optical model for Italian lakes focused on Landsat-8, Sentinel-2 and Sentinel-3. *Eur. J. Remote Sens.* 48, 17–32. <http://dx.doi.org/10.5721/EuJRS20154802>.
- Marsh, P., Hey, M., 1989. The flooding hydrology of Mackenzie Delta Lakes near Inuvik, N.W.T., Canada. *Arctic* 42, 41–49.
- Masek, J.G., Vermote, E.F., Saleous, N.E., Wolfe, R., Hall, F.G., Huemmrich, K.F., Gao, F., Kutler, J., Lim, T.K., 2006. A landsat surface reflectance dataset for North America, 1990–2000. *IEEE Geosci. Remote Sens. Lett.* 3, 68–72. <http://dx.doi.org/10.1109/LGRS.2005.857030>.
- McClelland, J.W., Holmes, R.M., Peterson, B.J., Amon, R., Brabets, T., Cooper, L., Gibson, J., Gordeev, V.V., Guay, C., Milburn, D., Staples, R., Raymond, P.A., Shiklomanov, I., Striegl, R., Zhulidov, A., Gurtovaya, T., Zimov, S., 2008. Development of a pan-Arctic database for river chemistry. *Eos. Trans. AGU* 89. <http://dx.doi.org/10.1029/2008EO240001>.
- McClelland, J.W., Townsend-Small, A., Holmes, R.M., Pan, F., Stieglitz, M., Khosh, M., Peterson, B.J., 2014. River export of nutrients and organic matter from the North Slope of Alaska to the Beaufort Sea. *Water Resour. Res.* 1823–1839. <http://dx.doi.org/10.1002/2013WR014722>. (Received).
- McClelland, J.W., Holmes, R.M., Peterson, B.J., Raymond, P.A., Striegl, R.G., Zhulidov, A.V., Zimov, S.A., Zimov, N., Tank, S.E., Spencer, R.G.M., Staples, R., Gurtovaya, T.Y., Griffin, C.G., 2016. Particulate organic carbon and nitrogen export from major Arctic rivers. *Glob. Biogeochem. Cycles* 30. <http://dx.doi.org/10.1002/2015GB005351>.
- McGuire, A.D., Hayes, D.J., Kicklighter, D.W., Manizza, M., Zhuang, Q., Chen, M., Follows, M.J., Gurney, K.R., McClelland, J.W., Melillo, J.M., Peterson, B.J., Prinn, R.G., 2010. An analysis of the carbon balance of the Arctic Basin from 1997 to 2006. *Tellus Ser. B Chem. Phys. Meteorol.* 62, 455–474. <http://dx.doi.org/10.1111/j.1600-0889.2010.00497.x>.
- Menard, H.L., Smith, S.M., 1966. Hypsometry of ocean provinces. *J. Geophys. Res.* 71, 4305–4325.
- Menken, K.D., Brezonik, P.L., Bauer, M.E., 2006. Influence of chlorophyll and colored dissolved organic matter (CDOM) on Lake reflectance spectra: implications for measuring Lake properties by remote sensing. *Lake Reservoir Manage.* 22, 179–190. <http://dx.doi.org/10.1080/07438140609353895>.
- Meon, B., Amon, R.M.W., 2004. Heterotrophic bacterial activity and fluxes of dissolved free amino acids and glucose in the Arctic rivers Ob, Yenisei and the adjacent Kara Sea. *Aquat. Microb. Ecol.* 37, 121–135. <http://dx.doi.org/10.3354/ame037121>.
- Mishra, N., Helder, D., Barsi, J., Markham, B., 2016. Continuous calibration improvement in solar reflective bands: Landsat 5 through Landsat 8. *Remote Sens. Environ.* 185, 7–15. <http://dx.doi.org/10.1016/j.rse.2016.07.032>.
- Neff, J.C., Finlay, J.C., Zimov, S.A., Davydov, S.P., Carrasco, J.J., Schuur, E.A.G., Davydova, A.I., 2006. Seasonal changes in the age and structure of dissolved organic carbon in Siberian rivers and streams. *Geophys. Res. Lett.* 33, 1–5. <http://dx.doi.org/10.1029/2006GL028222>.
- Novo, E.M.M., Hansom, J.D., Curran, P.J., 1989. The effect of sediment type on the relationship between reflectance and suspended sediment concentration. *Int. J. Remote Sens.* 10, 1283–1289. <http://dx.doi.org/10.1080/01431168908903967>.
- Olmanson, L.G., Bauer, M.E., Brezonik, P.L., 2008. A 20-year Landsat water clarity census of Minnesota's 10,000 lakes. *Remote Sens. Environ.* 112, 4086–4097.
- Olmanson, L.G., Brezonik, P.L., Finlay, J.C., Bauer, M.E., 2016. Comparison of Landsat 8 and Landsat 7 for regional measurements of CDOM and water clarity in lakes. *Remote Sens. Environ.* 185, 119–128. <http://dx.doi.org/10.1016/j.rse.2016.01.007>.
- Osburn, C.L., Stedmon, C.A., 2011. Linking the chemical and optical properties of dissolved organic matter in the Baltic – North Sea transition zone to differentiate three allochthonous inputs. *Mar. Chem.* 126, 281–294. <http://dx.doi.org/10.1016/j.marchem.2011.06.007>.
- Osterkamp, A.T.E., Viereck, L., Shur, Y., Jorgenson, M.T., Racine, C., Doyle, A., Boone, R.D., Osterkamp, T.E., Viereck, L., Shur, Y., Jorgenson, M.T., Racine, C., Doyle, A., Boone, R.D., 2000. Observations of Thermokarst and Its Impact on Boreal Forests in Alaska, U.S.A. INSTAAR, University of Colorado Stable. <http://www.jstor.org/stable/1552529> (REFERENCES Linked references are available on JSTOR for this article: Yo 32, 303–315).
- Pahlevan, N., Schott, J.R., 2013. Leveraging EO-1 to evaluate capability of new generation of landsat sensors for coastal/inland water studies. *IEEE J. Sel. Top. Appl. Earth Obs. Remote Sens.* 6, 360–374. <http://dx.doi.org/10.1109/JSTARS.2012.2235174>.
- Palmer, S.C.J., Kutser, T., Hunter, P.D., 2015. Remote sensing of inland waters: challenges, progress and future directions. *Remote Sens. Environ.* 157, 1–8. <http://dx.doi.org/10.1016/j.rse.2014.09.021>.
- Pavelsky, T.M., Smith, L.C., 2009. Remote sensing of suspended sediment concentration, flow velocity, and lake recharge in the Peace-Athabasca Delta, Canada. *Water Resour. Res.* 45, 1–16. <http://dx.doi.org/10.1029/2008WR007424>.
- Peacock, M., Freeman, C., Gauci, V., Lebron, I., Evans, C.D., 2015. Investigations of freezing and cold storage for the analysis of peatland dissolved organic carbon (DOC) and absorbance properties. *Environ. Sci.: Processes Impacts* 17, 1290–1301. <http://dx.doi.org/10.1039/C5EM00126A>.
- Pekel, J.-F., Cottam, A., Gorelick, N., Belward, A.S., 2016. High-resolution mapping of global surface water and its long-term changes. *Nature* 540, 418–422. <http://dx.doi.org/10.1038/nature20584>.
- Peterson, B., Hobbie, J.E., Corliss, T.L., 1986. Carbon flow in a tundra stream ecosystem. *Can. J. Fish. Aquat. Sci.* 43.
- Pokrovsky, O.S., Manasyapov, R.M., Loiko, S., Shirokova, L.S., Krickov, I.A., Pokrovsky, B.G., Kolesnichenko, L.G., Kopysov, S.G., Zemtsov, V.A., Kulizhsky, S.P., Vorobyev, S.N., Kirpotin, S.N., 2015. Permafrost coverage, watershed area and season control of dissolved carbon and major elements in western Siberian rivers. *Biogeosciences* 12, 6301–6320. <http://dx.doi.org/10.5194/bg-12-6301-2015>.
- Quibell, G., 1991. The effect of suspended sediment on reflectance from freshwater algae. *Int. J. Remote Sens.* 12, 177–182. <http://dx.doi.org/10.1080/01431169108929642>.
- Raymond, P.A., McClelland, J.W., Holmes, R.M., Zhulidov, A.V., Mull, K., Peterson, B.J., Striegl, R.G., Aiken, G.R., Gurtovaya, T.Y., 2007. Flux and age of dissolved organic carbon exported to the Arctic Ocean: a carbon isotopic study of the five largest arctic rivers. *Glob. Biogeochem. Cycles* 21, GB4011.
- Rodrigues, T., Alcántara, E., Watanabe, F., Imai, N., 2017. Retrieval of Secchi disk depth from a reservoir using a semi-analytical scheme. *Remote Sens. Environ.* 198, 213–228. <http://dx.doi.org/10.1016/j.rse.2017.06.018>.
- Runkel, R.L., Crawford, C.G., Cohn, T.A., 2004. Load estimator (LOADEST): a FORTRAN program for estimating constituent loads in streams and rivers. *USGS Techniques and Methods*.
- Schmidt, G., Jenkerson, C., Masek, J., Vermote, E., Gao, F., 2013. Landsat Ecosystem Disturbance Adaptive Processing System (LEDAPS) Algorithm Description. 2013 USGS.
- Sloncker, E.T., Jones, D.K., Pellerin, B.A., 2016. The new Landsat 8 potential for remote sensing of colored dissolved organic matter (CDOM). *Mar. Pollut. Bull.* 107, 518–527. <http://dx.doi.org/10.1016/j.marpolbul.2016.02.076>.
- Smith, L.C., Beilman, D.W., Kremenetski, K.V., Sheng, Y., Macdonald, G.M., Lammers, R.B., Shiklomanov, A.I., Lapshina, E.D., 2012. Short communication influence of permafrost on water storage in West Siberian peatlands revealed from a new database of soil properties. *Methods* 79, 69–79. <http://dx.doi.org/10.1002/ppp.735>.
- Spencer, R., Aiken, G., 2009. Utilizing chromophoric dissolved organic matter measurements to derive export and reactivity of dissolved organic carbon exported to the Arctic Ocean: A case study. *Geophys. Res. Lett.* 36, 1–6. <http://dx.doi.org/10.1029/2008GL036831>.
- Spencer, R.G.M., Coble, P.G., 2014. Sampling design for organic matter fluorescence analysis. In: Coble, P.G., Lead, J., Reynolds, D.M., Spencer, R.G.M. (Eds.), *Aquatic Organic Matter Fluorescence*. Cambridge Press, New York, NY, pp. 125–146.
- Spencer, R.G.M., Butler, K.D., Aiken, G.R., 2012. Dissolved organic carbon and chromophoric dissolved organic matter properties of rivers in the USA. *J. Geophys. Res. Biogeosci.* 117. <http://dx.doi.org/10.1029/2011JG001928>.
- Spencer, R.G.M., Aiken, G.R., Dornblaser, M.M., Butler, K.D., Holmes, R.M., Fiske, G., Mann, P.J., Stubbins, A., 2013. Chromophoric dissolved organic matter export from U.S. rivers. *Geophys. Res. Lett.* 40, 1575–1579. <http://dx.doi.org/10.1002/grl.50357>.
- Spencer, R.G.M., Mann, P.J., Dittmar, T., Eglinton, T.I., McIntyre, C., Holmes, R.M., Zimov, N.S., Stubbins, A., 2015. Detecting the signature of permafrost thaw in Arctic rivers. *Geophys. Res. Lett.* 11, 1–6. <http://dx.doi.org/10.1002/2015GL063498>.
- Stedmon, C.A., Amon, R.M.W., Rinehart, A.J., Walker, S.A., 2011. The supply and characteristics of colored dissolved organic matter (CDOM) in the Arctic Ocean: pan Arctic trends and differences. *Mar. Chem.* 124, 108–118. <http://dx.doi.org/10.1016/j.marchem.2010.12.007>.
- Striegl, R.G., Aiken, G.R., Dornblaser, M.M., Raymond, P.A., Wickland, K.P., 2005. A decrease in discharge-normalized DOC export by the Yukon River during summer through autumn. *Geophys. Res. Lett.* 32, L21413.

- Stubbins, A., Spencer, R.G.M., Mann, P.J., Holmes, R.M., McClelland, J.W., Niggemann, J., Dittmar, T., 2015. Utilizing colored dissolved organic matter to derive dissolved black carbon export by arctic rivers. *Front. Earth Sci.* 3, 1–11. <http://dx.doi.org/10.3389/feart.2015.00063>.
- Tank, S.E., Manizza, M., Holmes, R.M., McClelland, J.W., Peterson, B.J., 2012. The processing and impact of dissolved riverine nitrogen in the Arctic Ocean. *Estuar. Coasts* 35, 401–415. <http://dx.doi.org/10.1007/s12237-011-9417-3>.
- Tank, S.E., Striegl, R.G., McClelland, J.W., Kokelj, S.V., 2016. Multi-decadal increases in dissolved organic carbon and alkalinity flux from the Mackenzie drainage basin to the Arctic Ocean. *Environ. Res. Lett.* 11, 1–10. <http://dx.doi.org/10.1088/1748-9326/11/5/054015>.
- Toohey, R.C., Herman-Mercer, N.M., Schuster, P.F., Mutter, E.A., Koch, J.C., 2016. Multidecadal increases in the Yukon River Basin of chemical fluxes as indicators of changing flowpaths, groundwater, and permafrost. *Geophys. Res. Lett.* 43, 12,120–12,130. <http://dx.doi.org/10.1002/2016GL070817>.
- Vonk, J.E., Tank, S.E., Bowden, W.B., Laurion, I., Vincent, W.F., Alekseychik, P., Amyot, M., Billet, M.F., 2015. Reviews and syntheses: Effects of Permafrost Thaw on Arctic Aquatic. pp. 7129–7167. <http://dx.doi.org/10.5194/bg-12-7129-2015>.
- Walker, S.A., Amon, R.M.W., Stedmon, C.A., 2013. Variations in high-latitude riverine fluorescent dissolved organic matter: a comparison of large Arctic rivers. *J. Geophys. Res. Biogeosci.* 118, 1689–1702. <http://dx.doi.org/10.1002/2013JG002320>.
- White, D., Hinzman, L., Alessa, L., Cassano, J., Chambers, M., Falkner, K., Francis, J., Gutowski, W.J., Holland, M., Holmes, R.M., Huntington, H., Kane, D., Kliskey, A., Lee, C., McClelland, J., Peterson, B., Rupp, T.S., Straneo, F., Steele, M., Woodgate, R., Yang, D., Yoshikawa, K., Zhang, T., 2007. The arctic freshwater system: changes and impacts. *J. Geophys. Res.* 112, 1–21. <http://dx.doi.org/10.1029/2006JG000353>.
- Wickland, K.P., Neff, J.C., Aiken, G.R., 2007. Dissolved organic carbon in Alaskan boreal Forest: sources, chemical characteristics, and biodegradability. *Ecosystems* 10, 1323–1340. <http://dx.doi.org/10.1007/s10021-007-9101-4>.
- Wickland, K.P., Aiken, G.R., Butler, K., Dornblaser, M.M., Spencer, R.G.M., Striegl, R.G., 2012. Biodegradability of dissolved organic carbon in the Yukon River and its tributaries: seasonality and importance of inorganic nitrogen. *Glob. Biogeochem. Cycles* 26, 1–14. <http://dx.doi.org/10.1029/2012GB004342>.
- Woo, M.K., Thorne, R., 2003. Streamflow in the Mackenzie Basin, Canada. *Arctic* 56, 328–340.
- Worrall, F., Burt, T.P., 2010. Has the composition of fluvial DOC changed? Spatiotemporal patterns in the DOC-color relationship. *Glob. Biogeochem. Cycles* 24 (n/a-n/a). <https://doi.org/10.1029/2008GB003445>.
- Zhang, T., Osterkamp, T.E., Stamnes, K., 1997. Effects of climate on the active layer and permafrost on the North Slope of Alaska, U.S. *Permafr. Periglac. Process.* 8, 45–67. [http://dx.doi.org/10.1002/\(SICI\)1099-1530\(199701\)8:1<45::AID-PPP240>3.0.CO;2-K](http://dx.doi.org/10.1002/(SICI)1099-1530(199701)8:1<45::AID-PPP240>3.0.CO;2-K).